2

SiC Cage Like Based Materials

Patrice Mélinon
University of Lyon and CNRS
France

1. Introduction

SiC is a compound of silicon and carbon with a chemical formula SiC. Silicon carbide(SiC) as a material is the most promising for applications in which high-temperature, high-power, and high-frequency devices, catalyst support, high irradiation environments are needed. Naturally occurring SiC is found only in poor quantities that explains the considerable effort made in the industrial SiC engineering. At a first glad, silicon and carbide are close but a careful inspection reveals different properties leading to brothers at odds behavior. In well ordered stoichiometric compounds SiC adopts a tetrahedral bonding like observed in common semiconductors (zincblende and wurtzite are the most populars). The difference of electronegativities induces a ionicity which is not enough to promote NaCl or CsCl structures but enough to induce multipolar effects. These multipolar effects are responsible to the huge number of polytypes. This polytypism has numerous applications including quantum confinement effects and graphene engineering. In this chapter, special emphasis has been placed on the non stoichiometric compounds. Silicon architectures are based from sp^3 or more dense packing while carbon architectures cover a large spread of hybridization from sp to sp^3, the sp^2 graphite-like being the stable structure in standard conditions. When we gather silicon and carbon together one of the basic issue is: what is the winner? When silicon and carbon have the same concentration (called stoichiometric compound), the answer is trivial: "the sp^3" lattice since both the elements share this hybridization in bulk phase. In rich silicon phases, the sp^3 hybridization is also a natural way. However, a mystery remains when rich carbon compounds are synthesized. Silicon sp^2 lattice is definitively unstable while carbon adopts this structure. One of the solution is the cage-like structure (the fullerenes belongs to this family) where the hybridization is intermediate between sp^2 and sp^3. Other exotic structures like buckydiamonds are also possible. Special architectures can be built from the elemental SiC cage-like bricks, most of them are not yet synthesized, few are experimentally reported in low quantity. However, these structures are promising as long the electronic structure is quite different from standard phase and offer new areas of research in fuel cells (catalysis and gas storage), superconductivity, thermoelectric, optical and electronic devices…Moreover, the cage like structure permits endohedrally doping opening the way of heavily doped semiconductors strain free. Assembling elemental bricks lead to zeolite-like structures. We review the properties of some of these structures and their potential applications.

1.1 Carbon

Carbon has six electrons. Two of them will be found in the *1s* orbital close to the nucleus forming a compact core, the next two going into the 2s orbital. The remaining ones will be in two separate *2p* orbitals. The electronic structure of carbon is normally written $1s^2 2s^2 2p^2$. Contrary to silicon, germanium and tin, the unlikely promotion of an outer shell electron in a d state avoids the formation of compact structures. This clearly indicates that most of the chemical bonding involves valence electrons with *sp* character. In order to form two, three or four hybrid orbitals, the corresponding number of atomic orbitals has to be mixed within the framework of "hybridization concept". When the *s* orbital and all three *p* orbitals are mixed, the hybridization is sp^3. The geometry that achieves this is the tetrahedral geometry T_d, where any bond angle is 109.47^o (see fig. 1).

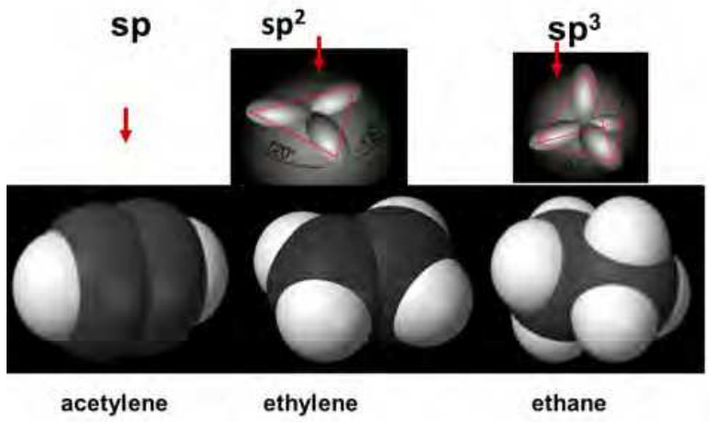

Fig. 1. elementary molecules corresponding to the three possible types of bonding. Acetylene C_2H_2 (sp bonding), ethylene C_2H_4 (sp^2 bonding) and ethane C_2H_6 (sp^3 bonding).

1.1.1 sp hybridization

When the s orbital and one p orbital are mixed, the hybridization is *sp*. The geometry is now linear, with the bond angle between the hybrid orbitals equal to 180^o. The additional p electrons which do not participate to the σ bonding (strong bond resulting from the overlap of hybrid orbitals) form the π bond, each orbital being perpendicular to the basal plane containing the σ bond. The *sp* carbon chains can present alternating single and triple bonds (polyyne)[α-carbyne] or only double bonds (polycumulene)[β-carbyne]; polyynes being more stable owing to the Peierls distortion (Kavan et al., 1995) which lifts the symmetry: double-double bond to simple-triple bond. The existence of carbyne is a subject of controversy and strictly speaking cannot be classified as a carbon allotrope. The existence of long linear chains becomes unlikely as soon as the length grows up. Crystalline carbyne must be unstable against virulent graphitization (sp to sp^2 transition) under normal conditions (Baughman, 2006). Up to date, the largest synthesized carbyne chain was $HC_{16}H$ (Lucotti et al., 2006) where terminated hydrogen ensures the stabilization of the carbyne. Even though, carbyne is the best prototype of the 1D network, the purity of the samples and the low chemical stability are the major hindrance for applications.

1.1.2 sp^2 hybridization

When the s orbital and two of the p orbitals for each carbon are mixed, the hybridization for each carbon is sp^2. The resulting geometry is the trigonal (hexagonal) planar geometry, with the bond angle between the hybrid orbitals equal to 120^0, the additional p electron is at the origin of the π band.

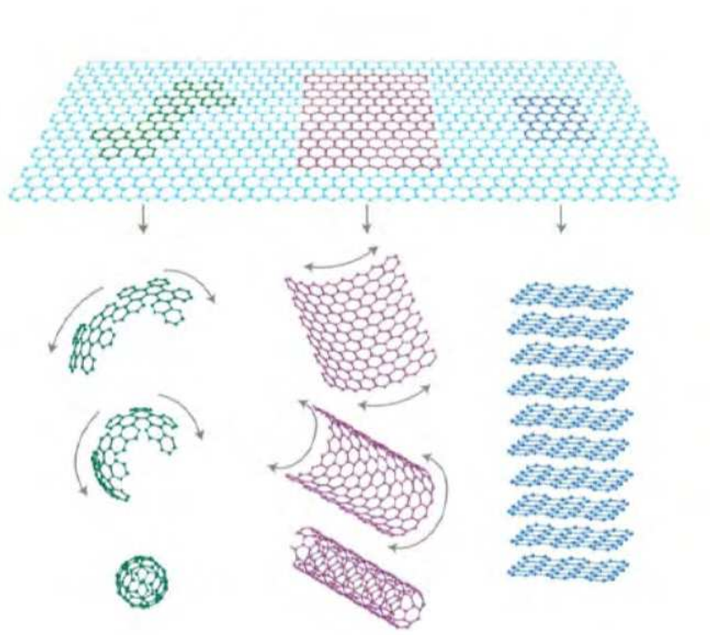

Fig. 2. how to build up graphite, nanotube or fullerene from a graphene sheet (after the original figure from Geim *et al* (Geim and Novoselov, 2007))

Graphene is of importance both for its unusual transport properties and as the mother for fullerene and nanotube families (figure 2). Graphene can be defined as an infinite periodic arrangement of (only six-member carbon ring) polycyclic aromatic carbon. It can be looked at as a fullerene with an infinite number of atoms. Owing the theoretical unstability of 2D networks, graphene sheets are stable over several microns enough for applications. Graphene has a two atom basis (A and B) per primitive cell arranged in a perfect hexagonal honeycomb. Except the center of the Brillouin zone Γ, the structure can be entirely described by symmetry with the particular setpoints **M**, **K** and **K'** related by the relationship **K**=-**K'**. For each atom, three electrons form tight bonds with neighbor atoms in the plane, the fourth electron in the p_z orbital does not interact with them leading to zero p_z orbital energy $E_z = 0$. It can be easily seen that the electron energy is zero at **K** and **K'**, graphene being a semiconductor with a zero bandgap. The most striking result is the linear relationship for the dispersion curve near **K** and **K'** . Since the effective mass is related to the second derivation of the energy, this implies a zero mass for the two electrons (one by site A and B). As a consequence, the classical picture of the Schrödinger equation must be replaced by the Dirac equation where Dirac spinors (two component wave function) are required in the mathematical description of the quantum state of the relativistic electron. This linear dispersion involving a multi degenerated states at the intersecting cones is broken by several ways: impurities, defects, interaction with two or

many graphene sheets (Partoens and Peeters, 2006)(Charlier et al., 1991), confinement effect (Nakada et al., 1996)(Son et al., 2006). After the degeneracy splitting, the dispersion tends to be parabolic with a "classical" effective mass. 3D graphite is formed by the stacking of graphene layers (Chung, 2002). The space group is $P6_3mmc - D_{6h}^{14}$ (number 194) with four atoms in the unit cell , two in position 2b at $\pm(00\frac{1}{4})$, and two in position $2d$ at $(\frac{2}{3}\frac{1}{3}\frac{1}{4})$. The two planes are connected by a translation $\mathbf{t} = (\mathbf{a}_1 + \mathbf{a}_2)/3 + \mathbf{a}3/2$ or by a C_6 rotation about the sixfold symmetry axis followed by a translation $\mathbf{a}3/2$ ($\mathbf{a}_i$ are the graphite lattice vectors)(fig. 3). This geometry permits the overlap of the π electrons leading to the π bonding. The electrons participating in this π-bonding seem able to move across these π-bonds from one atom to the next. This feature explains graphite's ability to conduct electricity along the sheets of carbon atom parallel to the (0001) direction just as graphene does.

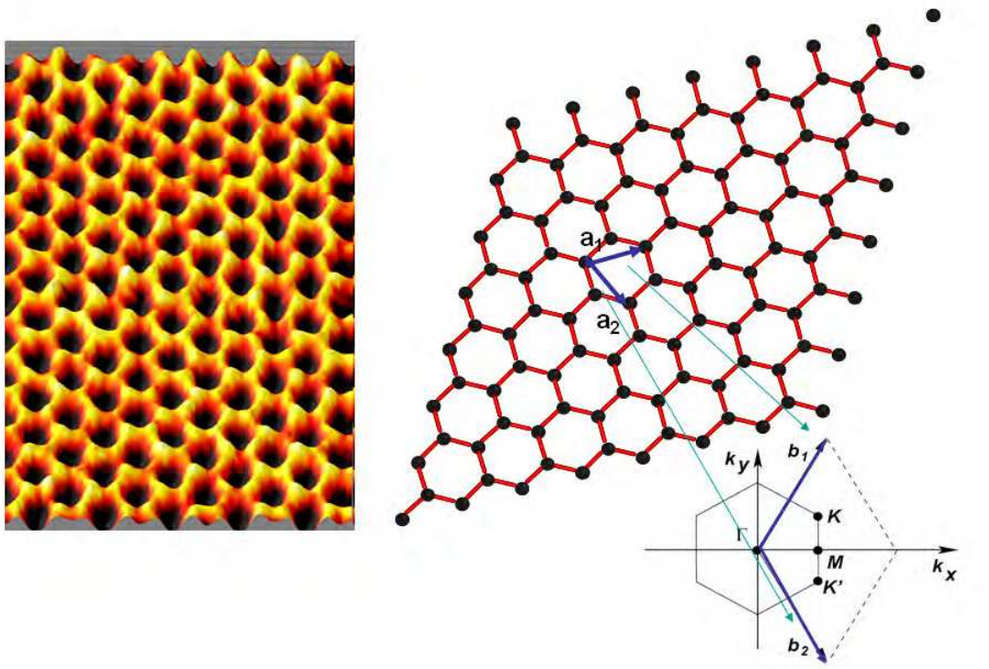

Fig. 3. left panel: Image of a single suspended sheet of graphene taken with a transmission electron microscope, showing individual carbon atoms (yellow) on the honeycomb lattice (after Zettl Research Group Condensed Matter Physics Department of Physics University of California at Berkeley). Right panel: ball and stick representation with unit vectors a_1 and a_2. The first 2D Brillouin zone is shown with the irreductible points (for further details about the figure see (Melinon and Masenelli, 2011)).

1.1.3 sp^3 hybridization

The most popular form is the cubic diamond (called diamond C-2), the second allotrope of carbon where each atom joined to four other carbons in regular tetrahedrons. The crystal structure is a face- centered cubic lattice with two atoms in the primitive cell. All the

C_2 units are in the staggered mode. The space group is $Fd\bar{3}m - O_h^7$ (number 227) with eight atoms in the conventional unit cell (two in the primitive cell). The two atoms are in position a (0,0,0) and (1/4,1/4,1/4) respectively with the coordinates of equivalent positions (0,0,0;0,1/2,1/2;1/2,0,1/2;1/2,1/2,0). The lattice constant is a=3.5669Å and the interatomic distance 1.5445Å (see figure 14). Contrary to graphite, the lack of the delocalized π band ensures an insulator character. Diamond is indeed a wide indirect band gap material with the $\Gamma_{25}^{'} - \Gamma_{15}$ transition of 7.3 eV and the indirect band gap of 5.45 eV. A (metastable) hexagonal polymorph of diamond (lonsdaleite) is also reported. The crystallographic description of this structure is $P6_3/mmc - D_{6h}^4$ (number 194) with four atoms per unit cell in position 4f $\pm$(1/3,2/3,1/16; 2/3,1/3,9/16). The lattice parameters are a=2.522Å and c=4.119Å, respectively. The main difference between the hexagonal structure and that of diamond is that in one quarter of the C_2 units the bonds are eclipsed. Other stacking sequence allows polytypism.

1.2 Silicon

Silicon has 14 electrons. Ten of them will be found in the *1s*, *2s* and *2p* orbitals close to the nucleus, the next two going into the *3s* orbital. The remaining ones will be in two separate *3p* orbitals. The electronic structure of silicon is written in the form $1s^2 2s^2 2p^6 3s^2 3p^2$. Because of this configuration, Si atoms most frequently establish sp^3 bonds (hybridization of a s orbital and three p orbitals) leading to tetrahedrally coordinated phases.

1.2.1 sp^3

The most stable phase in silicon is the cubic diamond. The structure is identical to the one discussed for carbon. The lattice constant is a=5.43Å. Each silicon is linked to the four neighboring atoms by 2.3515Å bond. Silicon diamond is an indirect band gap material. The $\Gamma_{25}^{'} - \Gamma_{15}$ transition is at 3.5 eV and the indirect band gap at 1.17 eV. As in carbon polytypism in hexagonal phase is also reported (combining eclipsed and staggered modes). Recently, a new metastable form has been isolated: the clathrate II (fig. 4. In the clathrates, the tetrahedra are mainly stacked in eclipsed mode while diamond is formed by stacking them in the staggered mode. Clathrate II is built by the coalescence of two Si_{28} and four Si_{20} per unit cell. It belongs to the same space group than the cubic diamond structure $Fd\bar{3}m$. Using the crystallographic notation, clathrate II is labeled Si-34 since we have $1/4(2 \times 28 + 4 \times 20) = 34$ atoms in the primitive cell. Such a structure is obtained by template one Si atom in the Si_5 basic sp^3 tetrahedron with Si_{28} cage, this latter having T_d point group symmetry. Si_{28} has four hexagons and share these hexagons with its four Si_{28} neighboring cages. The space filling needs additional silicon atoms in a tetrahedral symmetry forming Si_{20} cages. 85,7% of the membered rings are pentagons, implying that the electronic properties are sensitive to the frustration effect (contrary to bonding states, antibonding states contain one bonding node in odd membered rings). The difference in energy within DFT between Si-34 and Si-2 is of 0.06 eV per bond compared to 0.17 eV in the first metastable beta-tin structure .Clathrate II (Si-34) is obtained by heating the $NaSi_2$ silicide under vacuum or using a high pressure belt. Note that carbon clathrate is not yet synthesized as long as the precursor does not exist while the competition between clathrate and graphite (the most stable) phase operates. Several authors mentioned the Si clathrate potentiality for applications in optoelectronic devices. First of all, the wide band gap opening (around 1.9 eV) (Gryko et al., 2000; Melinon et al., 1998 ; Connetable et al., 2003; Connetable, 2003a ; Adams et al., 1994) ensures electronic transition

in the visible region and offers new potentialities in "all silicon" optoelectronic devices. Endohedrally doping is also possible. The Fermi level can be tailored by varying both the concentration and the type of atom inside the cage up to large concentration (>10%) without stress,vacancy-containing centers or misfits. For example, Fermi level easily lies at 0.5 eV above the conduction band minimum in n-doped clathrate (see fig. 13). Doped semiconducting clathrates (Tse et al., 2000) as candidates for thermoelectric power since endohedral atoms can effectively rattle around the cages.

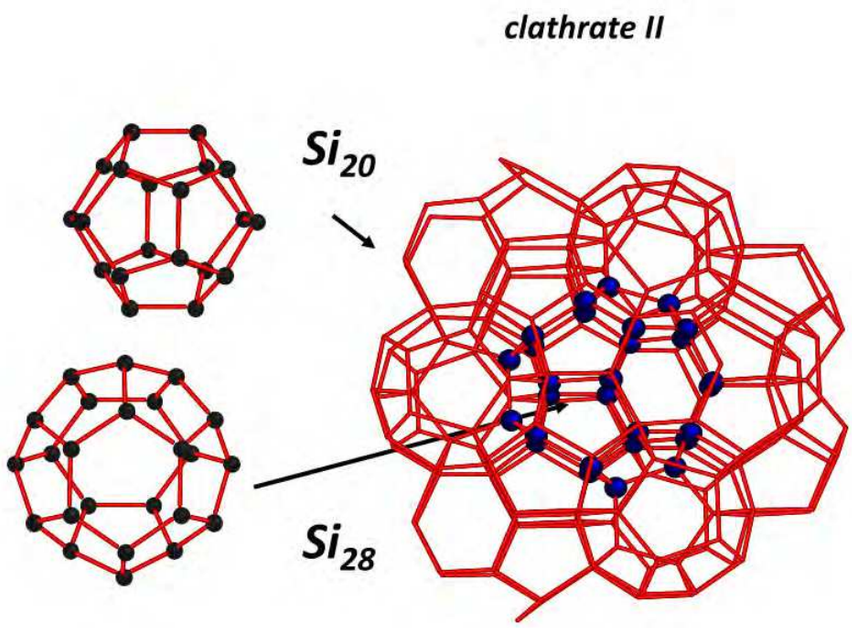

Fig. 4. a piece of clathrate II reported in silicon with a combination of Si_{28} and Si_{20}.

1.2.2 . . . and beyond

Contrary to carbon, the first transition observed in the excited state allows *spd* hybridizations. This is out of scope of this paper. *spd* hybridizations are reported in very small silicon clusters or in bulk phase at high pressure/temperature.

1.2.3 The case of sp^2

The elements with a principal quantum number equal to or greater than three are not capable of forming multiple bonds because of the considerable Pauli repulsion between the electrons of the inner shells. This golden rule summarizes the absence of π bonding in silicon. "Silicon graphite" is less stable than its diamond phase by 0.71 eV per atom (Yin and Cohen, 1984).

1.3 Silicon carbide

SiC is a compound of silicon and carbon with the net formula SiC. The first thing to note is that, from a bond point of view, chemical ordering is energetically favored: a *Si-C* bond (6.34 eV/atom (Kackell, 1994a;b)) is more stable by -0.35 eV/atom than the average of a *Si-Si* (4.63 eV/atom (Alfe et al., 2004)) and a C-C bond (7.35 eV/atom (Yin and Cohen, 1984)). The

applications are numerous (Choyke, 2004; Feng, 2004)) including the hardness (almost as hard as diamond), the extreme resistance to chemicals and radiation, a refractory compound, a tuning (wide) bandgap with high electron mobility, high breakdown electric field and good thermal conductivity. This is also a safe bio compatible compound.
Then, starting from a crystal with a perfect chemical order, introducing some disorder will cost two energetic contributions: a chemical enthalpy ΔH_{chem}, which is about 0.35 eV/atom in the ordered phase (Martins and Zunger, 1986) as mentioned above, and a strain enthalpy ΔH_{size}. Indeed, the large atomic size difference introduces a microscopic strain by incorporating *C-C* or *Si-Si* bonds while an ordered crystal is intrinsically strain free (we neglect the small variations in the atomic positions in polytypes). ΔH_{size} is of the same order of magnitude than the chemical contribution ($\Delta H_{size} \simeq 0.4$ eV/atom(Tersoff, 1994)). With a simple Arrhenius' law giving the measure of disorder, we can check that the occurence of *Si-Si* and/or *C-C* bonds is negligible over a large range of temperature. This differs from other compounds, such as *SiGe* where the chemical contribution is almost zero (a few meV negative (Martins and Zunger, 1986), meaning that *Si-Ge* bonds are slightly less favorable than *Si-Si* and *Ge-Ge* bonds and since *Si* and *Ge* have a comparable atomic size ($d_{Si-Si} = 2.35$ Å, $d_{Ge-Ge} = 2.445$ Å), the gain in strain energy is low enough to allow a significant chemical disorder.

1.4 The bottleneck: ionicity in SiC crystal

There is a charge transfer from *Si* to *C* in relation with the electronegativity difference between *Si* and *C* atoms (Zhao and Bagayoko, 2000). This charge transfer 0.66 $|e|$ (Segall et al., 1996) is affected by the d orbitals in silicon. The ionicity can be defined according to empirical laws stated by Pauling and Phillips or more accurate model within the calculated valence-charge asymmetry (Garcia and Cohen, 1993). Pauling made use of thermochemical arguments based from the electronegativities to determine the ionicity $f_i = 0.11$. Another standard picture based from the dielectric model first introduced by Phillips gives $f_i = 0.177$. However, Phillips' or Pauling's models do not take into account the crystal structure. This can be done in the simple static model where the ionicity parameter is defined in terms of the symmetric and antisymmetric parts of the atomic valence-charge density (Garcia and Cohen, 1993). According to the considered polytype, the static ionicity values f_i are 0.4724 (*2H*), 0.4718 (*3C*), 0.4720 (*4H*), and 0.4719 (*6H*). They do not change much from one polytype to another but they strongly differ from Pauling's ionicity (Wellenhofer et al., 1996). One possible consequence of the ionicity, depending on the structure, is the appearance of a spontaneous polarization.

1.5 Clathrate

No information about a *SiC* clathrate is available. Moriguchi *et al* (Moriguchi et al., 2000) and Wang *et al* (Wang et al., 2008) investigated the theoretical Si_xGe_{1-x} type II clathrate (see chapter 4). To minimize the homonuclear bonding *Si-Si* or *Ge-Ge* in pentagonal rings, non stoichiometric compounds (x=1/17,4/17,5/17,12/17,13/17,16/17) have been investigated. Some of these clathrate alloys with an ideal $Fd\bar{3}m$ symmetry are found to have direct band gap at the π/a(111) L point in the Brillouin zone which could be important for optoelectronic devices. However, the clathrate lattice needs a set of *Si-Si*, *Si-Ge* and *Ge-Ge* bonds which are close in distance values. This will be not the case in the *SiC* clathrate and questions the existence of such lattices in *SiC*.

1.6 Polytypism

name	space group	a	c	x	y	z	Wyckoff
3C-SiC	$F\bar{4}3m$ 216	4.368	-	(Si)0	0	0	*4a*
				(C)3/4	3/4	3/4	*4d*
3C-SiC	$P6_3mc$ 186	3.079	7.542	(Si)0	0	0	*2a*
				(C)0	0	1/4	*2a*
				(Si)1/3	2/3	1/3	*2b*
				(C)1/3	2/3	7/12	*2b*
				(Si)2/3	1/3	2/3	*2b*
				(C)2/3	1/3	11/12	*2b*
2H-SiC	$P6_3mc$ 186	3.079	5.053	(Si) 1/3	2/3	0	*2b*
				(C) 1/3	2/3	3/8	*2b*
4H-SiC	$P6_3mc$ 186	3.079	10.07	(Si) 0	0	0	*2a*
				(C) 0	0	3/16	*2a*
				(Si) 1/3	2/3	1/4	*2b*
				(C) 1/3	2/3	7/16	*2b*
6H-SiC	$P6_3mc$ 186	3.079	15.12	(Si) 0	0	0	*2a*
				(C) 0	0	1/8	*2a*
				(Si) 1/3	2/3	1/6	*2b*
				(C) 1/3	2/3	7/24	*2b*
				(Si) 2/3	1/3	1/3	*2b*
				(C) 2/3	1/3	11/24	*2b*

Table 1. The space group, unit cell lattice parameters (a and c), carbon and silicon fractional coordinates (x, y, z), multiplicities and Wyckoff positions of the sites for selected polytypes. A refinement of the positions is given by Bauer *et al* (Bauer et al., 1998)

Polytypism occurs when a structural change occurs within the same hybridization. In the case of SiC, we have some degrees of freedom in the way individual layers are stacked within a crystal structure, the driving force being the conservation of the chemical ordering. Silicon carbide exhibits a pronounced polytypism, the most simple polytypes are zinc-blende SiC (*3C-SiC*) and wurtzite (*2H-SiC*), the two structures correspond to the cubic and hexagonal diamonds when all the atoms are *Si* or *C* (see figure 5). The crystallographic data for selected polytypes are displayed in table 1

A single *Si-C* bilayer can be viewed as a planar sheet of silicon atoms coupled with a planar sheet of carbon atoms. The plane formed by a *Si-C* bilayer is known as the basal plane, while the crystallographic c-axis direction, also known as the stacking direction or the [0001] direction in the hexagonal lattice, is defined normal to the *Si-C* bilayer plane. All the *SiC* polytypes are classified following the arrangements of cubic or hexagonal *SiC* bilayers, stacking along the cubic [111] or the equivalent hexagonal [0001] direction.

The differences of cohesive energy in polytypes range in a few 0.01 eV (see table 2), state of the art *ab initio* calculations are not straightforward and out of range. Simple empirical potential (Ito and Kangawa, 2002; Ito et al., 2006), which incorporates electrostatic energies due to bond charges and ionic charges or Ising's model (Heine et al., 1992a) are reliable as depicted in table 2. According to Heine et al Heine et al. (1992a) one defines

$$\Delta E_{ANNNI,2H-SiC} = 2J_1 + 2J_3 \tag{1}$$

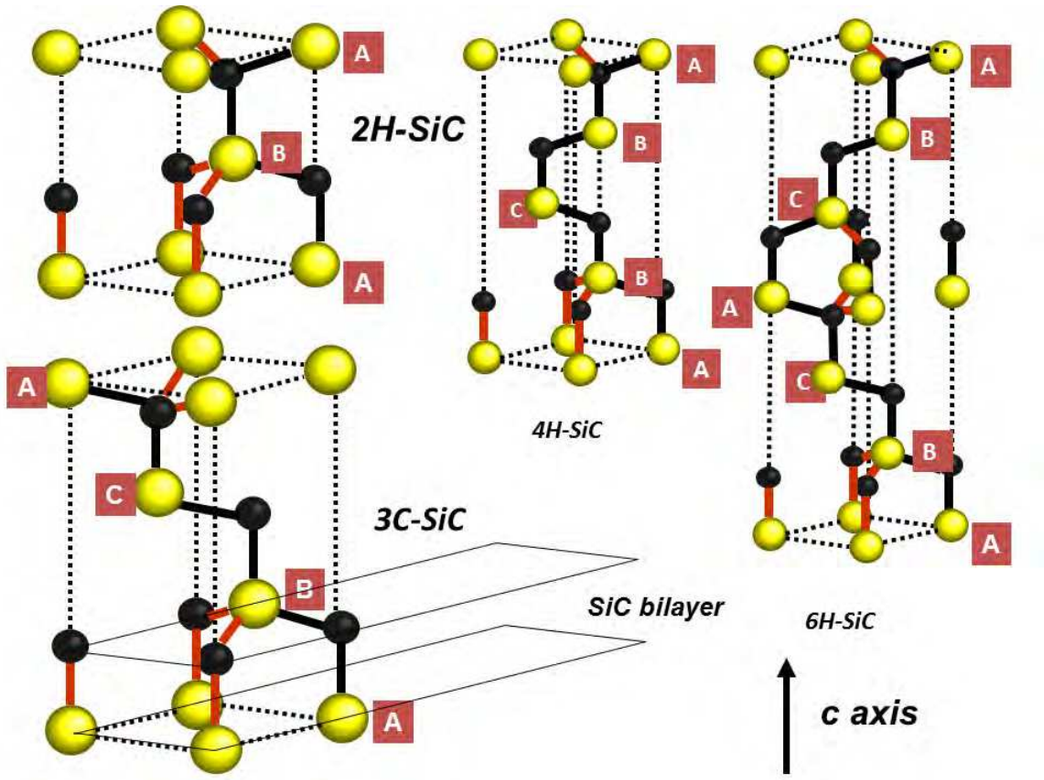

Fig. 5. ball and stick representation in three dimensional perspective of the first polytypes *2H-SiC*, *4H-SiC* and *6H-SiC* compared to *3C-SiC*. The chains structures which defined the stacking sequence are in dark color while selected *Si-C* bonds are in red color. The *SiC* bilayer is also shown. (Kackell, 1994a) after the original figure in reference (Melinon and Masenelli, 2011)

$$\Delta E_{ANNNI,4H-SiC} = J_1 + 2J_2 + J_3 \tag{2}$$

$$\Delta E_{ANNNI,6H-SiC} = \frac{2}{3}J_1 + \frac{4}{3}J_2 + 2J_3 \tag{3}$$

1.7 Application of the polytypism: quantum wells

Multi quantum wells first introduced by Esaki (Esaki and Chang, 1974) are potential wells that confines particles periodically, particles which were originally free to move in three dimensions. Esaki (Esaki and Chang, 1974) has defined a multi quantum well structure (*MQWS*) as a periodic variation of the crystal potential on a scale longer than the lattice constant, the most popular heterostructure being GaAs/AlAs superlattice (Sibille et al., 1990). *MQWS* devices are of prime importance in the development of optoelectronic devices. Unfortunately, these *MQWS* use elements which are not compatible with the basic "silicon" technology. This limits the integration of optoelectronic devices in complex chips. MQWS SiC based materials are under consideration keeping at mind that the stacking (a combination of eclipsed and staggered modes) of tetrahedra cell CSi_4 or SiC_4 strongly modify the bandgap value. This can be achieved controlling the stacking mode (polytypism assimilated to stacking

model	*3C-SiC*	*2H-SiC*	*4H-SiC*	*6H-SiC*	J_1	J_2	J_3
empirical[a]	0	2.95×10^{-3}	1.47×10^{-3}	0.92×10^{-3}	1.52	0.0	-0.05
DFT-GGA[a]	0	2.95×10^{-3}	-0.09×10^{-3}	-0.16×10^{-3}	1.55	-0.78	-0.08
DFT-LDA[b]	0	4.35×10^{-3}	-0.39×10^{-3}	-0.60×10^{-3}	4.85	-2.56	-0.50
DFT-LDA[c]	0	1.80×10^{-3}	-2.5×10^{-3}	-1.80×10^{-3}	2.00	-3.40	-0.20
DFT-LDA[d]	0	0.9×10^{-3}	-2.0×10^{-3}	-1.45×10^{-3}	1.08	-2.45	-0.18
FP-LMTO[e]	0	2.7×10^{-3}	-1.2×10^{-3}	-1.05×10^{-3}	3.06	-2.57	-0.35
DFT-LDA[f]	0	2.14×10^{-3}	-1.24×10^{-3}	-1.09×10^{-3}	2.53	-2.31	-0.40
DFT-LDA[g]	0	2.32×10^{-3}	-1.27×10^{-3}	-1.10×10^{-3}	2.71	-2.43	-0.39
DFT-GGA[g]	0	3.40×10^{-3}	-0.35×10^{-3}	-0.45×10^{-3}	3.72	-20.5	-0.33

Table 2. calculated energy difference (in eV) for selected polytypes within different models.
[a] from reference (Ito et al., 2006)
[b] from reference (Cheng et al., 1988)
[c] from reference (Park et al., 1994)
[d] from reference (Kackell, 1994a)
[e] from reference (Limpijumnong and Lambrecht, 1998)
[f] from reference (Lindefelt et al., 2003)
[g] from reference (Liu and Ni, 2005)

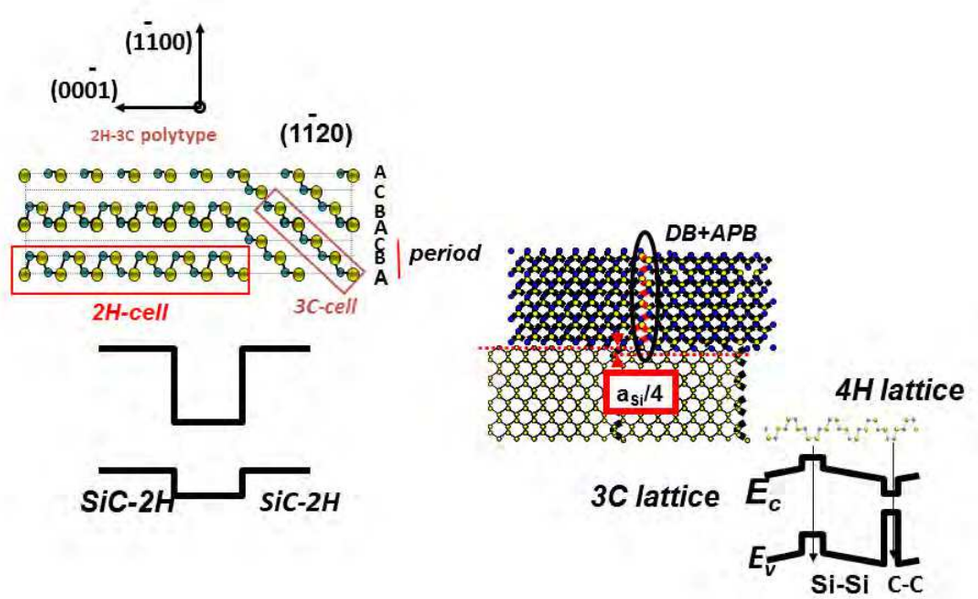

Fig. 6. left panel: illustration of the quantum well formed by the polytypism. Right panel: illustration of the quantum well formed by antiphase boundary (after the original figures in reference (Melinon and Masenelli, 2011) and references therein)

faults) or introduced extended defects such as antiphase boundary *APB*. The maximum value modulation in the potential corresponds with the bandgap difference between 3C-SiC and 2H-SiC $\Delta E_{max} = E_{g(3C-SiC)} - E_{g(2H-SiC)} \approx 1eV$ (see fig. 6).

1.7.1 Antiphase boundary

In the *APB*s (see fig. 6), the crystallographic direction remains unchanged but each side of the boundary has an opposite phase. For example, in *3C-SiC* described by *ABCABCABC* layers, one or two layer interruption in the stacking sequence gives the following sequence ABC**ABAB**CAB which is the alternance of *fcc/hcp/fcc* layers. The chemical ordering is disrupted with the appearance of *Si-Si* and *C-C* bonds. The associated bandgap modulation depends to several: the difference in valence, the difference in size of the atoms and the electrostatic repulsion in the *Si-Si* and *C-C* bond near the interface. *APB* formation is obtained when *3C-SiC* grows epitaxially on (100) silicon clean substrate (Pirouz et al., 1987). Deak *et al.* (Deak et al., 2006) reported a theoretical work where the expected tuning of the effective band gap ranges around 1 eV.

1.7.2 Cubic/hexagonal stacking

As mentioned above (fig. 6) , MQWS can be built from the stacking of different crystal structures of the same material as in wurtzite/zincblende heterostructures (Sibille et al., 1990).

1.8 Amorphous phase

1.8.1 Carbon

The maximum disorder can be observed in carbon where a large spread in hybridization and bonds coexist. Amorphous carbon can be rich in sp^2 bonding (vitreous carbon) or rich in sp^3 bonding (tetrahedral amorphous carbon and diamond like carbon).The properties of amorphous carbon films depend on the parameters used during the deposition especially the presence of doping such as hydrogen or nitrogen. Note that hydrogen stabilizes the sp^3 network by the suppression of dangling bonds.

1.8.2 Silicon

Since Si adopts a sp^3 hybridization, the amorphous state will be a piece of sp^3 network. The most popular model is the continuous random network (CRN) first introduced by Polk and Boudreaux (Polk and Boudreaux, 1973). As a consequence, five or seven-membered rings are introduced in the initial diamond lattice to avoid the occurrence of a long range order. Finally, dangling bonds are created at the surface and a spread in bond lengths and bond angles was observed (within 1% and 10%, respectively). Elemental a-Si cannot be used practically because of the dangling bonds, whose energy levels appear in the bandgap of silicon. Fortunately, this problem is solved by hydrogen incorporation which passive of the dangling bonds and participates to the relaxation of the stress in the matrix (a-Si:H). CRN models are hand-built models. A more rigorous approach is done by classical, semi empirical or *ab initio* calculations using molecular dynamics algorithms where a cluster of crystalline Si is prepared in a liquid state and rapidly quenched.

1.8.3 Silicon carbon

The major question is the extent of chemical disorder present in amorphous *SiC* network. There is not a consensus in the a-SiC network because of the huge number of parameters (chemical ordering, carbon hybridization, spread in angles and bonds, odd membered rings, dangling bonds . . .). The control of the chemical ordering in amorphous phase is the key point for applications in optoelectronics devices.

2. Cage-like molecules

2.1 Carbon: a rapid survey

2.1.1 Size range

Due to the high flexibility of the carbon atom, numerous isomers can be expected exhibiting complex forms such as linear chains (*sp* hybridization), rings , fused planar cycles (sp^2 hybridization), compact (sp^3 hybridization) and fullerene structures. We focus on particular structures in relation with complex architectures (zeolites) in bulk phase. From this point of view, fullerenes play a important role (Melinon et al., 2007).

2.1.2 Empty cages (fullerenes)

Starting with a piece of graphene (fully sp^2 hybridized) , the final geometry is given by a subtle balance between two antagonistic effects. One is the minimization of the unpaired electrons at the surface of the apex, the other is the strain energy brought by the relaxation due this minimization. The suppression of unpaired electrons is given by the standard topology (Euler's theorem). it is stated that (Melinon and Masenelli, 2011; Melinon and San Miguel, 2010) (and references therein)

$$2N_4 + N_5 = 12 \tag{4}$$

where N_i is the number of i membered- rings. The first case is $N_4 = 0$. This is achieved introducing at least and no more twelve pentagons ($N_5 = 12$), the number of hexagons (the elemental cell of the graphene) being $N_6 = 2i$ where i is an integer. Chemists claim that adjacent pentagons are chemically reactive and then introduce the concept of pentagonal rule (Kroto, 1987). Inspecting the Euler's relationship clearly indicates that the first fullerene with isolated pentagons is C_{60} with I_h symmetry. The mean hybridization is given by the π-Orbital Axis Vector Analysis

$$n = \frac{2}{1 - \frac{4\pi}{\sqrt{3}N}} \tag{5}$$

then taking graphene as reference for energy, the difference in energy writes

$$\Delta E = -3.1 \times 10^{-3}(\theta_{\pi\sigma} - \frac{\pi}{2})^2 \tag{6}$$

where

$$\sin(\theta_{\pi\sigma} - \frac{\pi}{2}) = \frac{2\pi^{1/2}N^{-1/2}}{3^{3/4}} \tag{7}$$

$\theta_{\pi\sigma}$ is the angle between π and σ orbitals.
The first (n=3, $N_6 = 0$) is the popular dodecahedron with I_h symmetry. Equation 5 gives a fully sp^3 hybridization. C_{20} is an open shell structure with a zero *HOMO-LUMO* separation. This structure is not stable as long the pentagons are fused and the strain energy maximum. Prinzbach *et al* (Prinzbach et al., 2000) prepared the three isomers according to different routes for the synthesis. The determination of the ground state in C_{20} is a subject of controversy as depicted in table 3 despite state of the art calculations.

method	geometry	E_{ring} -E_{bowl}	E_{ring}-$Ecage$	rank
[a]MP2/TZVd	optimized	2.08	0.03	bowl-cage-ring
[a]MP2/TZV2d	optimized	2.06	-0.66	cage-bowl-ring
[a]MP2/TZV2d1f	optimized	2.10	-0.54	cage-bowl-ring
[a]MP2/TZV2d1f	HF/6-31G$*$	2.61	0.69	bowl-cage-ring
[a]MR-MP2/TZV2d	MP2/TZV2d1f	2.42	-0.02	cage-bowl-ring
[a]MR-MP2/TZV2d1f	MP2/TZV2d1f	2.53	0.19	bowl-cage-ring
[a]MR-MP2/TZV2d1f	HF/6-31G$*$	3.00	1.27	bowl-cage-ring
[b]QMC	HF/6-31G$*$	1.1	2.10	bowl-ring-cage
[a]LDA/TZV2df//MP2/TZV2df		2.00	-1.0	cage-bowl-ring
[c]DFT B3LYP/6-311G$*$//B3LYP/6-311G*		0.4	1.9	ring-bowl-cage

Table 3. energy difference in eV ($\pm$ 0.5 eV) between the ring (expected ground state), bowl and cage against several methods which different treatments of correlation and polarization effects. The last column indicates the rank in stability
[a] after reference (Grimme and Muck-Lichtenfeld, 2002)
[b] after reference (Sokolova et al., 2000)
[c] after reference (Allison and Beran, 2004)

The *HOMO* state in I_h C_{20} has a G_u state occupied by two electrons, the closed-shell electronic structure occurs for C_{20}^{2+}. These high degeneracies are lifted by a Jahn Teller effect which distorts the cage (Parasuk and Almlof, 1991). Indeed after relaxation, the degeneracies can be removed lowering the total energy (-1.33eV in D_{2h} with respect to I_h (Wang et al., 2005)) and opening a *HOMO LUMO* separation (Sawtarie et al., 1994). It has been stated that dodecahedrane $C_{20}H_{20}$ first synthesized by Paquette's group (Ternansky et al., 1982) is stable with a heat of formation about 18.2 kcal/mol (Disch and Schulman, 1996). The dodecahedron is characterized by a 7.3 eV *HOMO* (h_u) *LUMO* a_g separation (Zdetsis, 2007). However, the *HOMO-LUMO* separation does not increases monotonically with the hydrogen content indicating particular stable structures such as $I_hC_{20}H_{10}$ with the same *HOMO-LUMO* separation than the fully saturated $I_hC_{20}H_{20}$ (Milani et al., 1996). Coming back to the equation 4. Another solution is $N_5 = 0$ giving $N_4 = 6$ (square rings as reported in in cyclobutane where the strain is maximum). The first polyhedron (equivalent to C_{60}) where isolated square rule is achieved is the hexagonal cuboctahedron with O_h symmetry (24 atoms) (the first Brillouin zone in fcc lattice, see fig. 15). However, the strain energy gained in squares is too large to ensure the stability as compared to D_6 C_{24} fullerene with (Jensen and Toftlund, 1993). C_{24} with $N_5 = 12$ is the first fullerene with hexagonal faces which presents in the upper symmetry a D_{6d} structure compatible with the translational symmetry (D_6 after relaxation). This is a piece of clathrate I described later (see fig. 13). Another fullerene T_dC_{28} has a ground state with a^5A_2 high-spin open-shell electronic state, with one electron in the a_1 molecular orbital and three electrons in the t_2 orbital (Guo et al., 1992) (see fig. 7). The close shell structure needs four electrons with a particular symmetry, three of them will be distributed on the t_2 orbital (*p-like* character) the last in the a_1 orbital (*s-like* character). This is the template of the carbon atom

making a sp^3 network. The four unpaired electrons make C_{28} behave like a sort of hollow superatom with an effective valence of 4. Introducing four hydrogen atoms outside in the T_d symmetry induces a close shell structure with the filling of the t_2 and a_1 states is checked by a *HOMO LUMO* separation of about 2.5 eV (Pederson and Laouini, 1993). $C_{28}H_4$ is the template of CH_4 leading to the hyperdiamond lattice. A closed shell structure is also done by the transfer of four electrons from a tetravalent embryo inside the cage. Since the size of C_{28} is low, this can be realized by incorporating one "tetravalent" atom inside the cage (X=Ti, Zr, Hf, U, Sc)(Guo et al., 1992)(Pederson and Laouini, 1993)(Makurin et al., 2001) (figure 7).

2.2 Silicon

2.2.1 Surface reconstruction

Theoretical determination of the ground-state geometry of Si clusters is a difficult task. One of the key point is the massive surface reconstruction applied to a piece of diamond (Kaxiras, 1990). The surface reconstruction was first introduced by Haneman (Haneman, 1961). The presence of a lone pair (dangling bond) destabilizes the network. One of the solution is the pairing. Since the surface is flat, this limits the possibility of curvature as reported in fullerenes. However, the surface relaxation is possible introducing pentagons (see for example references (Pandey, 1981; Himpsel et al., 1984; Lee and Kang, 1996; Xu et al., 2004; Ramstad et al., 1995)). This the key point to understand the stuffed fullerenes.

2.2.2 Stuffed fullerenes

Even though, the hybridization is fully sp^3 as in crystalline phase, I_h Si_{20} is not a stable molecule, the ground state for this particular number of Si atoms corresponding to two Si_{10} clusters (Sun et al., 2002; Li and Cao, 2000). Si_{20} cage -like structure is a distorted icosahedron with an open-shell electronic configuration as reported in C_{20} fullerene. Likewise, T_dSi_{28} fullerene is not a stable molecule. Starting from the T_d symmetry, a relaxation leads to a distorted structure which is a local minimum. Contrary to C_{28} (see above), the *HOMO* in T_d Si_{28} is formed by the t_2 symmetry level and the a_1 symmetry level for *LUMO* (Gao and Zheng, 2005). Si in Si_{28} is more atomic like than C in C_{28} (Gong, 1995). Except these discrepancies, Si_{28} can be stabilized by four additional electrons coming from four hydrogen atoms outside or a tetravalent atom inside. However the cage diameter is too big for an efficient coupling with one tetravalent atom, even for the bigger known (uranium). Consequently, a single metal atom cannot prevent the T_h Si_{28} cage from puckering and distortion. This problem can be solved introduced a molecule which mimics a giant tetravalent atom, the best being T_dSi_5 referred to Si_5H_{12} which has a perfect T_d symmetry (figure 7). T_dSi_5 has a completely filled twofold degenerated level at the *HOMO* state (Gao and Zheng, 2005). The final cluster $Si_5@Si_{28}$ is noted Si_{33} . Si_{33} has two classes of network: one corresponding to the fullerene family which exhibits T_d symmetry and can be deduced from a piece of clathrate, and one corresponding to the surface reconstruction of the *Si* crystal having a T_{d1} space group (Kaxiras, 1990). The difference is the exact position of Si_5 inside the Si_{28} cage. Since the total energy in the two isomers are very close, this emphasizes the concept of "superatom" with a large isotropy. The hybridization picture is not the good approach and a charge transfer picture seems more appropriate. Stuffed fullerene Si_{33} is found to be unreactive in agreement with the *HOMO LUMO* separation.

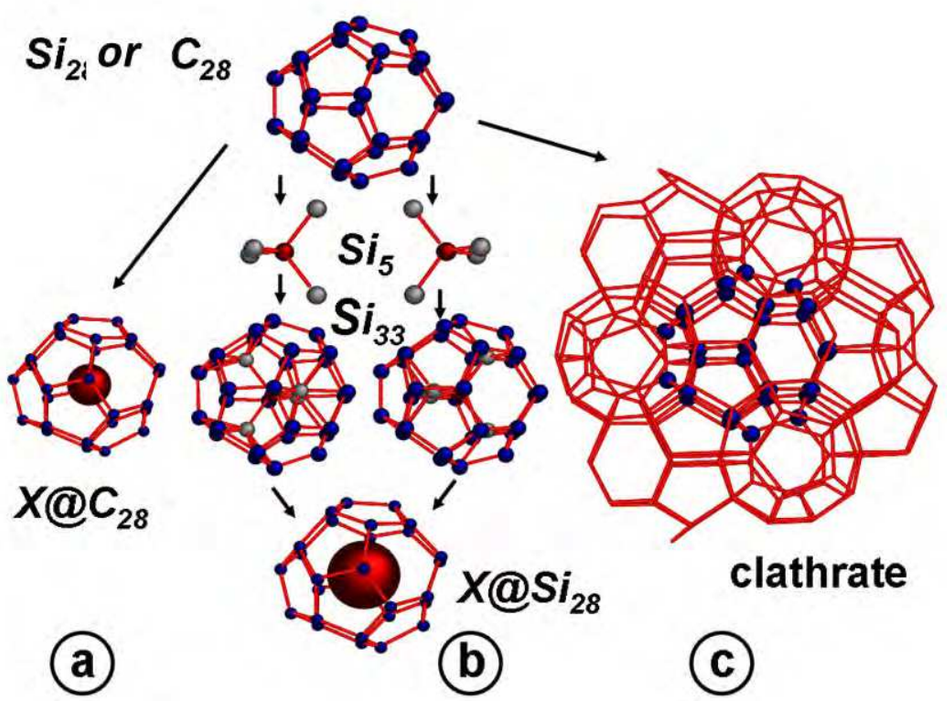

Fig. 7. scenario the an efficient doping in C_{28} and Si_{28} cage. Contrary to carbon , silicon needs a giant tetravalent atom. (a) endohedrally doped C_{28} cage stable for a tetravalent atom (uranium for example). (b) endohedral doping in Si_{28} cage by incorporation of two Si_5 clusters. The two isomers have roughly the same cohesive energy within DFT-GGA framework. (after the original figure in reference (Melinon and Masenelli, 2009)

2.3 Silicon carbon

The driving force in bulk is the chemical ordering. Inspecting equation 4 gives two possibilities: fullerene or cuboctahedron families. The first leads to non chemical ordering, the second to chemical ordering with a large stress because of four fold rings.

2.3.1 Quasi chemical ordering: buckydiamond

Starting from a spherically truncated bulk diamond structure, relaxation gives (Yu et al., 2009) a buckydiamond structure where the facets are reconstructed with the same manner as *Si* or *C* surfaces (figure 8). The inner shells have a diamond-like structure and the cluster surface a fullerene-like structure. Even though, the chemical ordering is not strictly achieved at the surface, the ratio of C-C and Si-Si bonds due to pentagons decreases as the cluster size increases. The reconstruction presents some striking features with the surface reconstruction in bulk phase.

2.3.2 Non chemical ordering: core shell structure

Most of the experiments done in SiC nanoclusters indicate a phase separation which does not validate a buckyball structure even though the buckyball is expected stable. The kinetic pathway plays an important role and the final state strongly depends to the synthesis: route

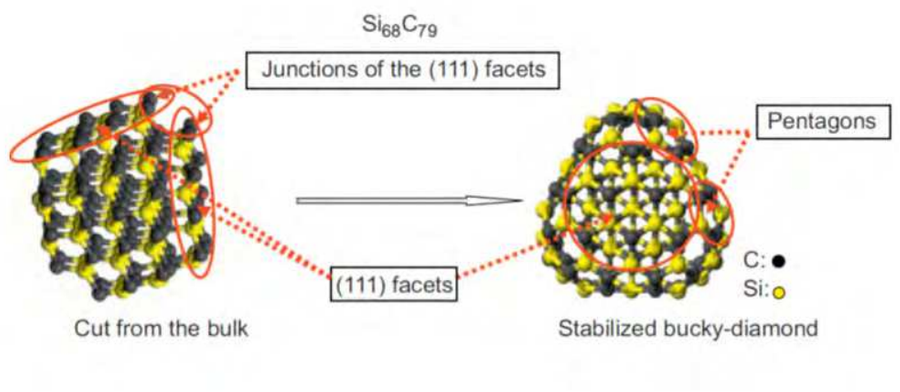

Fig. 8. A piece of $\beta - SiC$ (truncated octahedron with (111) facets) and the final geometry after relaxation. The more spherical shape indicates a massive reconstruction of the surface. The inner shell remains sp^3 hybridized with a nearly T_d symmetry while the surface presents a set of pentagons and hexagons which is common in fullerenes. The original figure is in reference (Yu et al., 2009)

chemical or physical. The key point is the stoichiometry. When carbon and silicon are in the same ratio, one observes a complete phase separation with a core shell structure for the corresponding clusters.

2.3.3 Non chemical ordering: amorphous structure

Figure 9 displays the structure of the cluster starting with a core shell structure. It is found that for Si core ($Si_n@C_m$, $Si_m@C_n$), Si atoms are dragged to the exterior and the relaxation process leads to a strong distortion, with some Si and C atoms bonded. The spread in angles indicate a complexity in the hybridization close to the amorphous state. One of the key point is the phase separation in small nanoclusters as depicted on figure 9 where Si-Si, C-C bonds coexist with Si-C bonds at the interface of Si- and C-rich regions, respectively.

3. SiC cage like

For a low percentage of silicon, carbon adopts a geometry close to the fullerene where a few Si-atoms (less than twelve) are substituted to carbon atoms in the fullerene structure (Ray et al., 1998; Pellarin et al., 1999). The effect of the stoichiometry can be studied by selective laser evaporation. One takes advantage of the difference in cohesive energy (bonding) between Si-Si and C-C bonds within a a parent SiC stoichiometric cluster. As a function of time during laser irradiation, sequential evaporation of Si atoms (or molecules) yield is more efficient than carbon evaporation leading to pure carbon clusters after total evaporation of silicon atoms. Inspecting the different size distributions deduced from a time of flight mass spectrometer against time reveals sequentially different structures: stoichiometric

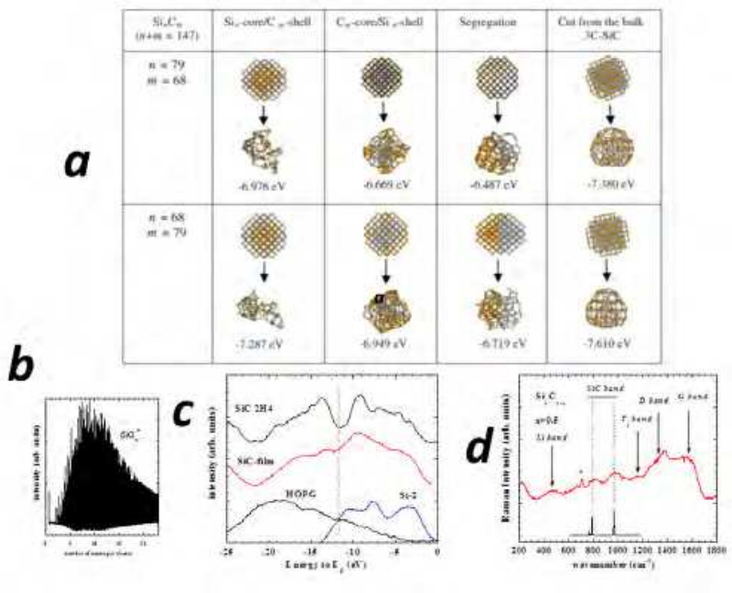

Fig. 9. (a) Relaxation of different hypothetic structures. from left to right: ($Si_n@C_m$, $Si_m@C_n$) showing the complex "amorphous structure" and the lack of the spherical shape, $C_n@Si_m$, $C_m@Si_n$ showing the C-rich region in the core, the spherical shape being preserved, the non chemical ordering phase showing the strong relaxation and the incomplete chemical ordering due to the large barriers in the diffusion and the buckyball structure. The cohesive energy per atom is also displayed. The original figure is in reference (Yu et al., 2009). (b) size distribution of SiC nanoparticles prepared in a laser vaporization source. A cluster assembled film is subsequently prepared by low energy cluster beam deposition. (c) valence band spectra deduced from XPS spectroscopy and (d) Raman band spectra showing silicon- and carbon-rich local phases. To guide the eye, the Raman modes and their symmetries in the crystal are given. The Raman spectrum of a *2H-SiC* is also displayed. the spread in bond lengths and bond angles due to the multiple hybridization is well illustrated by the broad bands in Raman and XPS spectra. In a crude approximation, these bands reflect the *p-DOS* in the infinite lattice. The original figure is in reference (Melinon et al., 1998a)

clusters, heterofullerenes ($C_{2N} - nSi_n$) and C_{2N} fullerenes, respectively. The figure 10 displays the landscape of the phase transition between a pure fullerene like structure up to a piece of adamantane, the stoichiometry being the tuning parameter.

Figure 11 displays the symbolic ball and stick models for two heterofullerenes with one silicon atom, respectively, C_{60} being the mother. Inspecting the region near the gap (HOMO-LUMO region)shows the analogy with doped semiconductors by substitution. HOMO-LUMO separation in heterofullerenes are weakly affected by Si atoms compared to pure C_{60} fullerenes. The Si-related orbitals (dashed lines) can be described in terms of defect levels. Because Si and C belong to the same column, Si atom plays the role of co doping with two acceptor-like and donor-like levels. For two Si atoms substituted in C_{60}, the mechanism is the same excepted the splitting of each donor level in two levels.

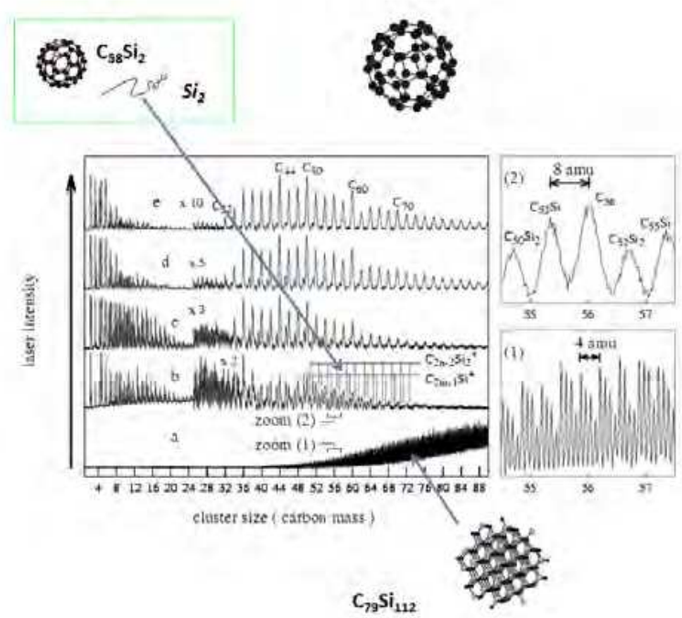

Fig. 10. Photoionization mass spectra of initial stoichiometric SiC clusters for increasing laser fluences. The time of flight mass spectrometer can be equipped with a reflectron device. Experimental details are given in the reference (Pellarin et al., 1999). The horizontal scale is given in equivalent number of carbon atoms. (a) High resolution one-photon ionization mass spectrum obtained in the reflectron configuration. (b) to (e) Multiphoton ionization mass spectra obtained at lower resolution without the reflectron configuration to avoid blurring from possible unimolecular evaporation in the time of flight mass spectrometer. The right part of the spectra (b) to (e) have been magnified for a better display. In (b) the heterofullerene series with one and two silicon atoms are indicated. Insets (1) and (2) give a zoomed portion of spectra 3(a) and 3(b). The 4 a.m.u. separation between Si_nC_m mass clumps is shown in (1) and the composition of heterofullerenes (8 a.m.u. apart) is indicated in (2). The mass resolution in (2) is too low to resolve individual mass peaks as in (1) (after the original figure (Pellarin et al., 1999)).

3.1 C_{60} functionnalized by Si

Because of the closed shell structure, C_{60} packing forms a Van der Waals solid. Many research have been done to functionalize the C_{60} molecules without disrupt the π-π conjugation (Martin et al., 2009). Most of the methods are derived from chemical routes. Silicon atom can be also incorporated between two C_{60} molecules (Pellarin et al., 2002) by physical route. Bridging C_{60} is evidenced in free phase by photofragmentation experiments (Pellarin et al., 2002) and in cluster assembled films by EXAFS spectroscopy performed at the Si K edge (Tournus et al., 2002). Such experiments are compatible with a silicon atom bridging two C_{60} molecules. Different geometries are tested and the best configuration for the fit corresponds to a silicon atom bridging two C_{60}. Figure 11 displays the configuration where two nearest C_{60} face the silicon atom with a pentagonal face. In this case, we have ten neighbors located at 2.52Å as compared to four neighbors located at 1.88Å in SiC carbide. The geometry around silicon suggests an unusual bonding close to intercalated graphite rather than a sp^3 basic set.

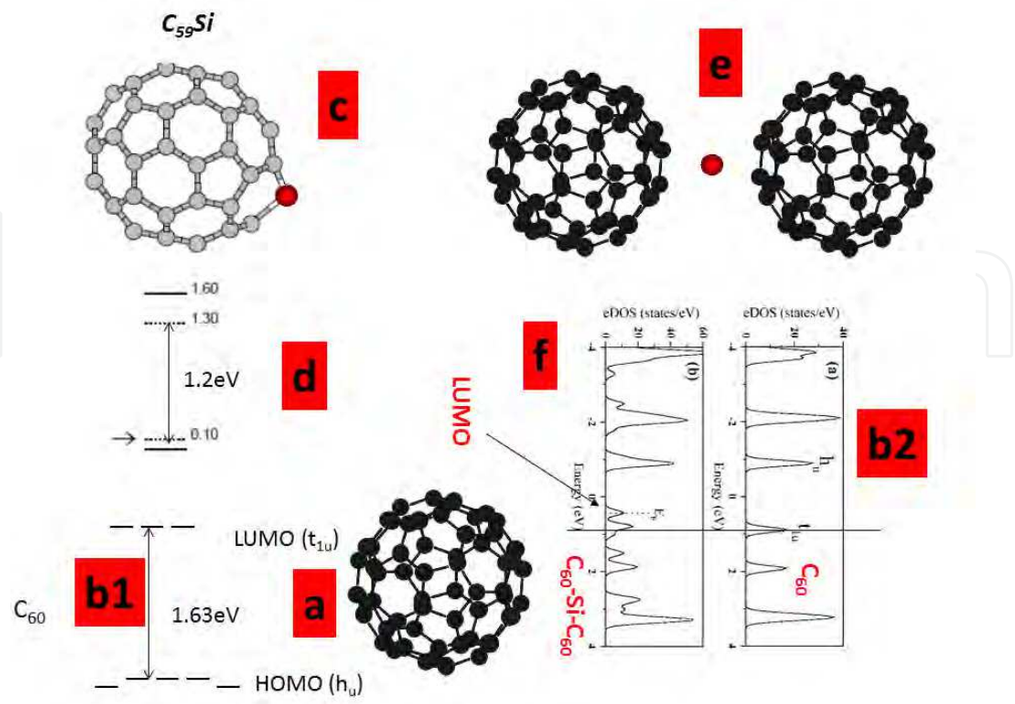

Fig. 11. a:symbolic ball and stick representation of C_{60}.b1,2: selected energy levels near the HOMO-LUMO C_{60} region. c: symbolic ball and stick representation of SiC_{59} , the geometries are deduced from DFT-LDA calculations and relaxed following the standard conjugate gradient scheme (see reference (Ray et al., 1998)). The red sphere is the silicon atom. d: selected energy levels near the SiC_{59} HOMO-LUMO region. Full lines and dotted lines indicate the carbon- and silicon-related orbitals, respectively. Taking only carbon-related orbitals, the HOMO-LUMO separation is respectively 1.68 eV,1.60 eV for C_{60}, $C_{59}Si$ and respectively. The arrow gives the HOMO LUMO separation. In this way, the HOMO-LUMO separation is 1.2 eV in $C_{59}Si$. e: ball and stick representation of C_{60}-Si-C_{60} (after reference (Tournus et al., 2002)).f: selected energy levels near the HOMO-LUMO C_{60}-Si-C_{60} region

4. Zeolites: expanded-volume phases of SiC

There is a entanglement between empty or stuffed fullerenes and zeolite lattices. The interest on these nanocage based materials has been impelled by their potentialities in different domains from which we mention the optoelectronic engineering, integrated batteries, thermoelectric power, hard materials or superconductivity. These expanded-volume phases 12 are formed by triplicate arrangement of a combination of these elemental cages (fullerenes for example). The doped expanded-volume phases offer new advantages

i) A large flexibility in the nature and the strength of the coupling between the guest atom and the host cage following the valence and the size of the guest atom.

ii) a large flexibility in doping (n or p) as long no significant stress is observed for a very large concentration (up to 10%). Two kinds of open structures are under consideration. The first is the Kelvin's lattice (named bitruncated cubic honeycomb or "sodalite" in zeolite language formed by a regular stacking of truncated octahedra which are Archimedean solids with 14

faces (8 regular hexagons and 6 squares), 36 edges, and 24 vertices leading to the net formula $(AB)_{12}$ (A=C,Si, B=C,Si) the second the clathrate formed by a stacking of fullerenes.
From a topological point of view, the clathrate is the best candidate to the complex mathematical problem of minimal partitioning of space into equal volumes is given by the Weare-Phelan conjecture. However, SiC is not stable in clathrate structure because of the odd parity in five fold rings.

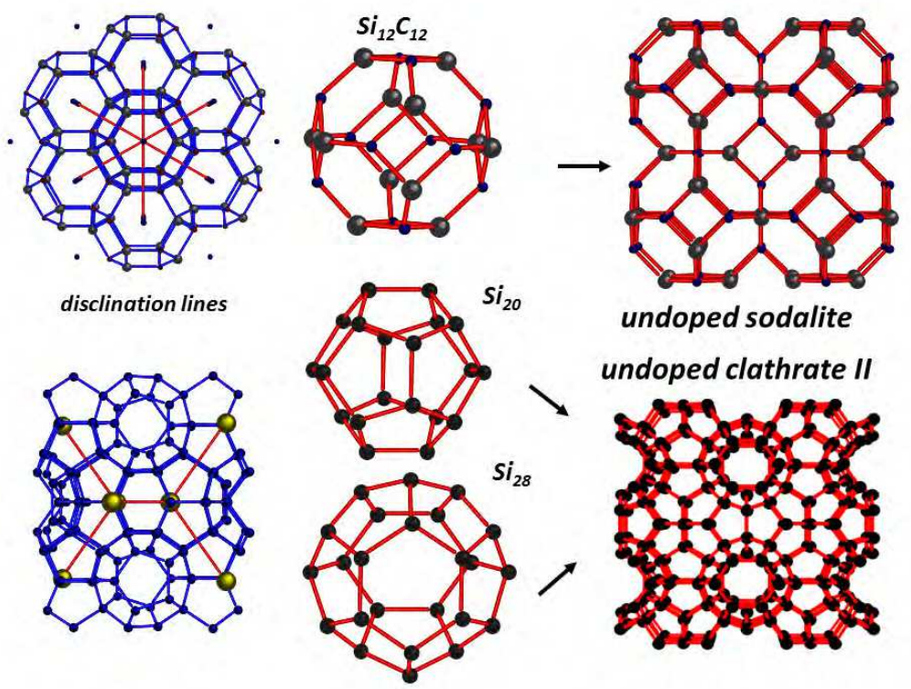

Fig. 12. sodalite structure compared to clathrate II. Both lattices are expanded volume phases but sodalite presents even membered rings allowing a chemical ordering. The "disclination lines" (for the definition see (Melinon and San Miguel, 2010)) display the lattice formed by endohedral atoms in the case of doped structures.

4.1 Clathrates: a survey

Clathrates are 3D periodic networks of dodecahedral fullerenes with either X_{24} or X_{28} polyhedral cage-like nanoclusters respectively. In type-I clusters, only X_{20} and X_{24} can be found, while the so-called type-II phases contain X_{20} and X_{28}. The silicon clusters are sharing faces, giving rise to full sp^3 -based networks of slightly distorted tetrahedra.

4.2 Endohedral doping

Elemental electronic devices need n and p doping. n-type doping of diamond is one of the most important issues for electronic application of diamond and remains a great challenge. This is due to the fact that the solubility of donor impurities in the diamond lattice is predicted to be low. Highly conductive silicon obtained by heavy doping is limited by the maximum solubility of the dopants provided it can be kept in solid solution. Beyond this limit precipitates or vacancy-containing centers are reported. Endohedral doping is one of the solution as long as the Fermi level can be tailored by varying both the concentration

and the type of atom inside the cage. This is well illustrated in clathrate Si-46, $Na_8@Si-46$ and $Ba_8@Si-46$ (see figure 13) (the notation $Ba_8@Si-46$ indicates eight barium atoms for

name	space group	a	x	y	z	Wyckoff
X-34	$Fd\bar{3}m$ origin at center $\bar{3}m$	a	1/8	1/8	1/8	*8a*
			0.782	0.782	0.782	*32e*
			0.817	0.817	0.629	*96g*
X-46	$Pm\bar{3}m$ origin at $4\bar{3}m$	a	1/4	0	1/2	*6c*
			0.1847	0.1847	0.1847	*16i*
			0	0.3088	0.1173	*24k*
sodalite	$Pm\bar{3}n$	b	1/4	0	1/2	*6c*
			1/4	1/2	0	*6d*

Table 4. The space group, unit cell lattice parameters (a and c) in Å, carbon and silicon fractional coordinates (x, y, z), multiplicities and Wyckoff positions of the sites for selected clathrates I and II and sodalite.

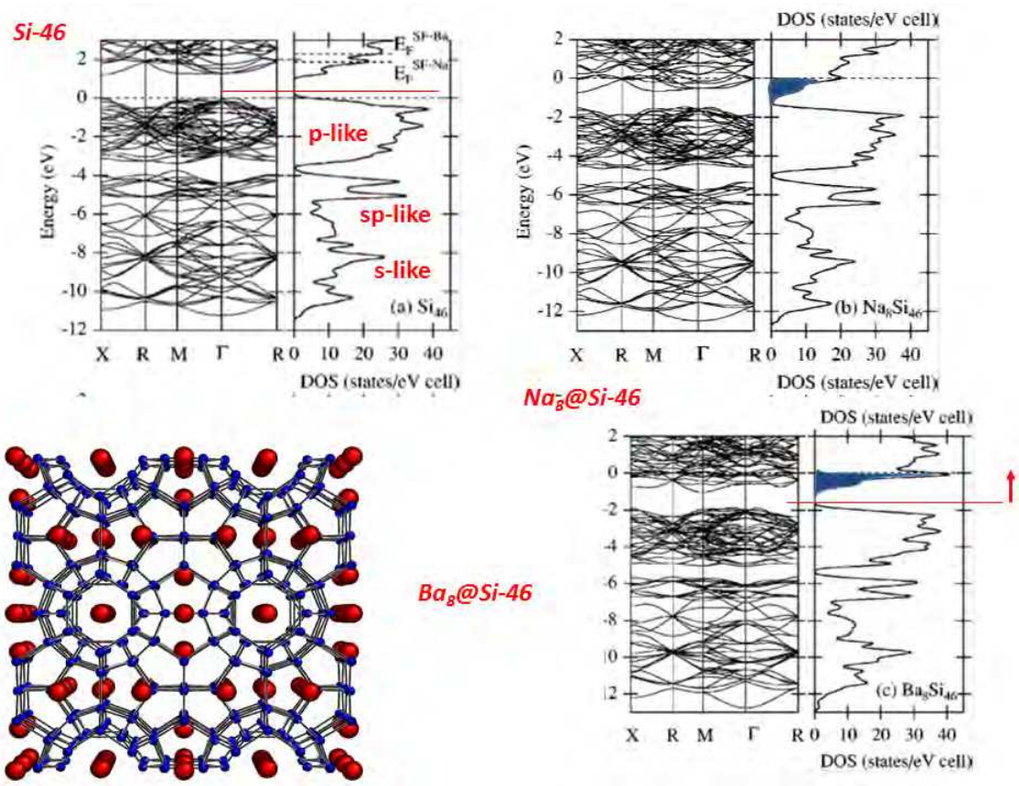

Fig. 13. Band structures and density of states for (a) *Si-46* , (b) $Na_8@Si-46$, and (c) $Ba_8@Si-46$. The ball and stick representation displays the $X_8@Si-46$ lattice (X=Na,Ba). Density of states are calculated using 0.1 eV Gaussian broadening of the band structure. Energy is measured from the top of the valence band or the Fermi level, which is denoted by horizontal broken lines. The blue filled region displays the occupied states in the conduction band. Note the strong hybridization of the Barium states responsible of the high density of states at E_F in $Ba_8@Si-46$. This sample is superconductor with a $T_c = 8K$. (after the original figure from (Moriguchi et al., 2000a)).

46 silicon atoms corresponding to the number of Si atoms in the primitive cell, in this case all the cages Si_{20} and Si_{24} are occupied . Note that the decoupling between the host lattice (the clathrate) and the guest lattice (doping atoms) is the key point for thermoelectric power generation and superconductivity applications in cage-like based materials. Moreover, the cage-like based materials present an interesting feature due to the great number of the atoms inside the elemental cell. This is well illustrated in the figure showing two {111} cleavage planes in a diamond lattice. The first (labeled "diamond") displays the well known honeycomb lattice with a nice "open" structure. The second corresponds to the clathrate with a more complex structure. This partially explained why the cage-like structures contrary to diamond (unlike hardness, which only denotes absolute resistance to scratching) the toughness is high and no vulnerable to breakage (Blase et al., 2004)(fig. 14).

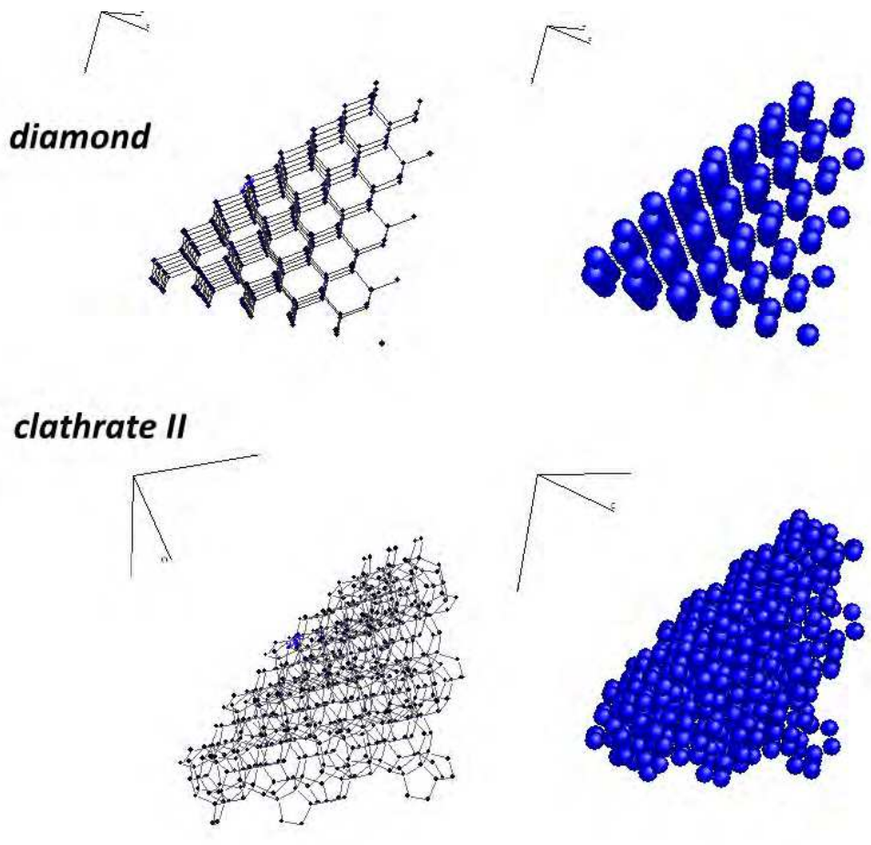

Fig. 14. cleavage plane along 111 projection in diamond and clathrate structures showing the large difference in atomic density. The toughness is high and no vulnerable to breakage in clathrate despite a weaker bonding (10% lower than in diamond phase). Fore more details see reference (Blase et al., 2004).

4.3 Carbon clathrate

The carbon clathrate synthesis is a major challenge since no precursor exists except intercalated graphite and doped fullerites. The competition between $sp - sp^2$ and sp^3 phases avoids the natural formation of carbon clathrate at high pressure and/or temperature. Numerous authors have attempted the synthesis without success.

4.4 Silicon clathrate

In the absence of angle-resolved photoemission data, the band structure of clathrates has been discussed on the basis of tight-binding (Adams et al., 1994) and *ab-initio* density functional (Hohenberg and Kohn, 1964; Kohn, 1999) (DFT) calculations (Melinon et al., 1998 ; Moriguchi et al., 2000; Saito and Oshiyama, 1995; Adams et al., 1994). In particular, DFT studies within the local density approximation (Kohn and Sham, 1965) (LDA) predict (Moriguchi et al., 2000a; Adams et al., 1994) that the Si-34 phase displays a "nearly-direct" band gap which is ~ 0.7 eV larger than the one of bulk Si-2 diamond. Such a large band gap has been attributed to the presence of pentagons which frustrates the formation of completely bonding states between Si-*3p* orbitals at the top of the valence bands, thus reducing the *p*-band width.

4.5 Silicon carbon: topology

As mentioned above, chemical ordering is the driving force and expanded volume phases as candidates need odd parity in rings. No clathrate lattice excepted may be non stoichiometric compounds are expected.

4.6 Sodalite and other simple phases

The Atlas of Zeolite Framework Types (Ch. Baerlocher, L.B. McCusker and D.H. Olson, Elsevier, Amsterdam, 2007) contains 176 topological distinct tetrahedral TO_4 frameworks, where T may be Si. Some examples are illustrated in figure 15. The crystallographic data are given in table 5. From a theoretical point of view, the SiO_4 unit cell can be replaced by SiC_4 or CSi_4. The most compact is the sodalite mentioned above. Within DFT-LDA calculations, the difference in energy between the sodalite and the cubic 3C-SiC is 0.6 eV per SiC units (16.59 eV per SiC in 3C-SiC within the DFT-LDA framework (Hapiuk et al., 2011)). Among the huge family of structures, ATV is more stable with a net difference of 0.52 eV per SiC units (see table 6). This energy is small enough to take in consideration cage-like SiC based materials and the potentiality for its synthesis. This opens a new field in doping as long the elements located at the right side in the periodic table induce a p-like doping while elements at the left side induce a n-like doping. Moreover, one can takes advantage to the wide band opening in expanded-volume phases. Inspecting the table reveals a direct gap in ATV structure within DFT-LDA level. This structure is the most stable and presents interesting features for optical devices in near UV region. Even though DFT/LDA has the well-known problem of band-gap underestimation, it is still capable of capturing qualitatively important aspects by comparison between 3C- and other structures. Open structures have a promising way as long as the structures could be synthesized by chemists.

name	space group	a	x	y	z	Wyckoff
ATV	*ABm2*[number 39]	a=5.788				
		b=9.236				
		c=5.007				
	Si		0.849	.25	0.692	*4c*
	Si		0.651	0.099	0.192	*8d*
	C		0.849	0.25	0.308	*4c*
	C		0.651	0.0.099	0.808	*8d*
AFI	*P6cc* [number 184]	a=8.4669				
		b=a				
		c=5.003				
	Si		0.455	0.122	0.192	*12d*
	C		0.545	0.878	0.808	*12d*
LTA	$Fm\bar{3}c$ [number 226]	a=b=c=10.2129				
	Si		0	0.0924	0.1848	*96i*
	C		0	0.1848	0.0924	*96i*
VFI	$P6_3cm$ [number 185]	a=b=11.6075				
		c=5.0307				
	Si	0.4227	0	0.063	*6c*	
	Si		0.1786	0.512	0.563	*12d*
	C		0.5773	0	0.937	*6c*
	C		0.8214	0.488	0.437	*12d*
ATO	$R\bar{3}$ [number 148]	a=b=12.942				
		c=3.0284				
	Si		0.1992	0.251	0.250	*18f*
	C		0.0518	0.251	0.250	*18f*

Table 5. The space group, unit cell lattice parameters (a and c) in Å, carbon and silicon fractional coordinates (x, y, z), multiplicities and Wyckoff positions of the sites for selected zeolites. 3C-SiC and sodalite are displayed in tables 1 and 4 respectively. The lattice parameters are deduced from DFT-LDA calculations within SIESTA code and standard procedure (Hapiuk et al., 2011). The coordinates are in reference (Demkov et al., 1997).

name	energy difference per SiC units	bandgap	type	d_{SiC}
3C-SiC	0	1.376	indirect	1.88
ATV	0.524	1.949	direct $\Gamma - \Gamma$	(1.842-1.923)
sodalite	0.598	1.718	indirect	1.881
VFI	1.065	1.063	indirect	(1.889-1.904)
LTA	1.126	1.586	indirect	(1.883-1.887)
ATO	1.210	1.035	indirect	(1.908-2.104)

Table 6. energy difference to the ground state per SiC in eV, LDA bandgap, transition and neighboring distance at the DFT-LDA level. Calculations were done within the density functional theory DFT in the local density approximation . The Perdew-Zunger parametrization of the Ceperley-Alder homogeneous electron gas exchange-correlation potential was used. The valence electrons were treated explicitly while the influence of the core electrons and atomic nuclei was replaced by norm-conserving Trouiller-Martins pseudo potentials factorized in Kleinman-Bylander form. For the doping elements, pseudo potentials were generated including scalar relativistic effects and a nonlinear core correction was used to mimic some of the effects of the d shell on the valence electrons. We employed the SIESTA program package which is a self-consistent pseudo potential code based on numerical pseudo atomic orbitals as the basis set for decomposition of the one-electron wave functions (Hapiuk et al., 2011).

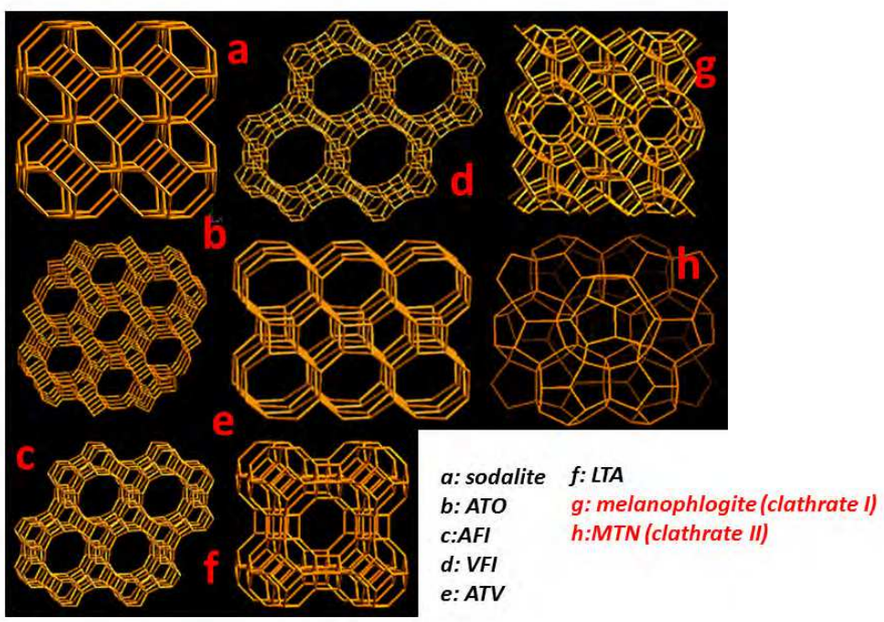

Fig. 15. selected zeolites forms. (a) sodalite with single 6-rings in ABC sequence with single 4-rings or 6-2 rings. (b) ATO with single 4- or 6-rings. (c) AFI with single 4- or 6-rings. (d) VFI with single 6-rings. (e) ATV with single 4-rings. (f) LTA with double 4-rings, (single 4-rings), 8-rings or 6-2 rings. (g) melanophlogite with 5-rings (clathrate I see above). (h) MTN with 5-rings (clathrate II see text). The two clathrate forms are unlikely because the breakdown of the chemical ordering. Fore more details see the "Commission of the International Zeolite Association (IZA-SC)" http://izasc-mirror.la.asu.edu/fmi/xsl/IZA-SC/ft.xsl

5. Conclusion: future research

Most of the SiC forms are nearly sp^3 hybridized. Inspecting the new architectures based from cage-like cells do not reveal anyway another hybridization. The silicon make one's mark, other hybridizations are definitively discarded. However, the topology of the open-structures like zeolites is still interesting since its offer a set of unique features: low density, tunable bandgap (direct or indirect), endohedral doping hydrogen storage …This is enough to promote a renewable interest and some efforts for their synthesis. In addition, all the properties attributed to the open structures in cage-like based materials are universal since the driving force is the topology, namely the symmetry of the cage and the symmetry of the whole lattice. Same features are observed in other binary compounds such as GaAs or ZnO. In addition, the inspection of the bulk and molecular phases underlines the prominent role of the pentagons where the chemical ordering is broken. This is the striking difference between C,Si and SiC.

6. References

Kavan,L.Hlavatý,J. Kastner,J. and Kuzmany,H. (1995) *Electrochemical carbyne from perfluorinated hydrocarbons: synthesis and stability studied by Raman scattering*, *Carbon* 33,1321 –1329.

Baugham,R.H. (2006) *Dangerously Seeking Linear Carbon Science* 312,1009 –1110.

Lucotti, A. Tommasini, M. Zoppo, M. Del Castiglioni, C. Zerbi, G. Cataldo, F. Casari, C.S. Bassi, A. Li Russo, V. Bogana, M. and Bottani, C.E. (2006). *Raman and SERS investigation of isolated sp carbon chains* , *Chemical Physics Letters*417, p78–82.

Geim,AK. and Novoselov,K.S. (2007) *The rise of graphene,Nature Materials* 6,183–191.

Partoens,B. and Peeters,F.M. (2006) *From graphene to graphite: Electronic structure around the K point,Phys. Rev. B* 74,075404 1–11.

Charlier,J.C. Michenaud,J.P. Gonze,X. and Vigneron,J.P. (1991) *Tight-binding model for the electronic properties of simple hexagonal graphite,Phys. Rev. B* 44,13237–13249.

Nakada,K. Fujita,M. Dresselhaus,G. and Dresselhaus,M.S. (1996) *Edge state in graphene ribbons: Nanometer size effect and edge shape dependence,Phys. Rev. B* 54,17954–17961.

Son,Y.W. Cohen,M.L. and Louie,S.G. (2006) *Energy Gaps in Graphene Nanoribbons,Phys. Rev. Lett.* 97,216803 1–4.

Chung,D.D.L. (2002) *Review Graphite,J. of Mat. Sci.* 37,1475 –1489.

Melinon,P. and Masenelli B., *From Small Fullerenes to Superlattices: Science and Applications*, Pan Stanford Publishing Pte Ltd (2011)

Gryko, J., McMillan, P., Marzke, R., Ramachandran, G., Patton, D., Deb, S. and Sankey, O. (2000) *Low-density framework form of crystalline silicon with a wide optical band gap Phys. Rev. B* 62,R7707–R7710.

Adams,G.B. O'Keeffe,M. Demkov,A.A. Sankey,O.F. and Huang,Y. (1994) *Wide-band-gap Si in open fourfold-coordinated clathrate structures,Phys. Rev. B* 49,8048–8053.

Melinon, P., Keghelian, P., Blase, X., Le Brusc, J., and Perez, A. (1998). *Electronic sig- nature of the pentagonal rings in silicon clathrate phases: Comparison with cluster- assembled films Phys. Rev. B* 58,12590–12593.

Connetable, D., Timoshevskii, V., Masenelli, B., Beille, J., Marcus, J., Barbara, B., Saitta, A., Rignanese, G., Melinon, P., Yamanaka, S. and Blase, X. (2003) *Superconduc- tivity in Doped sp3 Semiconductors: The Case of the Clathrates Phys. Rev. Lett.* 91,247001 1–4.

Connetable,D. (2003) *Ph.D. thesis, Universite of Lyon, LPMCN batiment Brillouin Do maine de la Doua 69622 Villeurbanne France*

Tse, J.S. Uehara,K. Roussea u,R. Ker,A. Ratcliffe,C.L. White,M.A. and Mackay,G. *Structural principles and amorphouslike thermal conductivity of Na-doped silicon clathrates Phys. Rev. Lett.* 85,114–117.

Yin,M.T. and Cohen,M.L. (1974) *Structural theory of graphite and graphitic silicon, Phys. Rev. B* 29,6996–6998.

Kackell,P. and Wenzien,B. and Bechstedt,F. *Electronic properties of cubic and hexagonal SiC polytypes from ab initio calculations Phys. Rev. B* 50,10761–10768.

Kackell,P. and Wenzien,B. and Bechstedt,F. (1994) *Influence of atomic relaxations on the structural properties of SiC polytypes from ab initio calculations Phys. Rev. B* 50,10761–10768.

Alfe,D; and Gillan,M.J. and Towler,M.D. and Needs,R.J.(2004) *Diamond and β-tin structures of Si studied with quantum* Monte Carlo *calculations Phys. Rev. B* 70,214102 1–8.

W. J. Choyke, Hiroyuki Matsunami, G. Pensl *Silicon Carbide: recent major advances* Springer Verlag,Berlin Heidelberg (2004). *Phys. Rev. B* 44,17037–17046.

Zhe Chuan Feng, *SiC power materials: Devices and applications*,Springer Verlag,Berlin Heidelberg (2004). *Phys. Rev. B* 44,17037–17046.

Martins, J. L. and Zunger, A. (1986) *Stability of ordered bulk and epitaxial semiconductor alloys Phys. Rev. Lett.* 56,1400–1404.

Tersoff , J. (1994) *Chemical order in amorphous silicon carbide Phys. Rev. B* 49,16349–16352.

G L Zhao and D Bagayoko (2000) *Electronic structure and charge transfer in 3*C *and 4*H-S*i*C *New Journal of physics* 2,16 1–12.

Segall, M. D., Shah, R., Pickard, C. J. and Payne. *Population analysis of plane-wave electronic structure calculations of bulk materials Phys. Rev. B* 54,16317–16320.

Garcia,A. and Cohen,M.L. (1993) *First-principles ionicity scales.* I. C*harge asymmetry in the solid state Phys. Rev. B* 47,4215–4220.

Wellenhofer,G. and Karch,K. and Pavone,P. and Rossler,U. and Strauch,D. (1996) *Pressure dependence of static and dynamic ionicity of* S*i*C *polytypes Phys. Rev. B* 53,6071–6075.

Moriguchi,K; and Munetoh,S. and Shintani,A. (2000) *First-principles study of* $Si_{34-x}Ge_x$ *clathrates: Direct wide-gap semiconductors in* S*i*-G*e alloys Phys. Rev. B* 62,7138–7143.

Wang,H. and Chu,W. and Jin,H. and Xiong,Y. (2008) *Atomistic simulation of* S*i*G*e clathrate alloys Chem. Phys.* 344,299–308.

Ito, T. and Kangawa, Y. (2002). *An empirical potential approach to wurtzitezinc blende structural stability of semiconductors Journal of Crystal Growth* 235,149–153.

Ito, T., Sano, K., Akiyama, T. and Nakamura, K. (2006). *A simple approach to polytypes of SiC and its application to nanowires Thin Solid Films* 508,243–246.

Heine, V., Cheng, C. and Needs, R. (1992a). *Computational study into the origin of SiC polytypes Materials Science and Engineering, B: Solid-State Materials for Advanced Technology* B11,55–60.

Esaki, L. and Chang, L. (1974). *New Transport Phenomenon in a Semiconductor Superlattice Phys. Rev. Lett.* 33,495–498.

Bauer, A., Kraulich, J., Dressler, L., Kuschnerus, P., Wolf, J., Goetz, K., Kackell, P., Furthmuller, J. and Bechstedt, F. (1998) *High-precision determination of atomic positions in crystals: The case of 6H- and 4H-SiC Phys. Rev. B* 57,2647–2650.

Sibille, A., Palmier, J.,Wang, H. and Mollot, F. (1990). *Observation of Esaki-Tsu Negative Differential Velocity in GaAs/AlAs Superlattices Phys. Rev. Lett.* 64,52–55.

Polk, D. and Boudreaux, D. (1973). *Tetrahedrally Coordinated Random-Network Structure Phys. Rev. Lett.* 31,92–95.

Pirouz, P., Chorey, C. and Powell, J. (1987). *Antiphase boundaries in epitaxially grown β-SiC Appl. Phys. Lett.* 4,221–223.

Deak, P., Buruzs, A., Gali, A. and Frauenheim, T. (2006). *Strain-Free Polarization Superlattice in Silicon Carbide: A Theoretical Investigation Phys. Rev. Lett.* 96,236803 1–4.

Cheng, C., Needs, R. and Heine, V. (1988). *Inter-layer interactions and the origin of SiC polytypes J. Phys. C: Solid State Phys.* 21,1049–1063.

Park, C., Cheong, B., Lee, K. and Chang, K. (1994). *Structural and electronic properties of cubic, 2H 4H and 6H SiC Phys. Rev. B* 49,4485–4493.

Limpijumnong, S. and Lambrecht, W. (1998). *Total energy differences between SiC poly- types revisited Phys. Rev. B* 57,12017–12022.

Lindefelt, U., Iwata, H., Oberg, S. and Briddon, P. (2003). *Stacking faults in 3C-, 4H-, and 6H-SiC polytypes investigated by an ab initio supercell method Phys. Rev. B* 67,157204 1–12.

Liu, Z. and Ni, J. (2005). *Layered growth modelling of epitaxial growth processes for SiC polytypes J. Phys.: Condens. Matter* 17,5355–5366.

Melinon, P., Masenelli, B., Tournus, F. and Perez, A. (2007). *Playing with carbon and silicon at the nanoscale Nature Materials* 6,479–490.

P.Melinon and A. San Miguel (2010). *From silicon to carbon clathrates : nanocage materials Chapter in the vol. "Clusters and Fullerenes" The HANDBOOK OF NANOPHYSICS* Taylor & Francis. (K.Sattler guest editor). ISBN: 9781420075540.

Kroto, H. (1987). *The stability of the fullerenes cn, with n = 24, 28, 32, 36, 50, 60 and 70 Nature* 329,529–531.

Prinzbach, H., Weiler, A., Landenberger, P., Wahl, F., Worth, J., Scott, L., Gelmont, M., Olevano, D. and Issendorf, B. (2000). *Gas-phase production and photoelectron spectroscopy of the smallest fullerene, C20 Nature* 407,60–63.

Parasuk, V. and Almlof, J. (1991). *C20: the smallest fullerene? Chem. Phys. Lett.* 184,187–190.

Wang, Z., Lian, K., Pan, S. and Fan, X. (2005b). *A Path from Ih to C1 Symmetry for C20 Cage Molecule Journal of Computational Chemistry* 26,1279–1283.

Grimme, S., and Muck-Lichtenfeld, C. (2002). *Structural isomers of C20 Revisited: The Cage and Bowl are Almost Isoenergetic CHEMPHYSCHEM* 2,207–209.

Sokolova, S., Luchow, A. and Anderson, J. (2000). *Energetics of carbon clusters C20 from all-electron quantum monte carlo calculations Chemical Physics Letters* 323,2229–233.

Allison, C. and Beran, K. (2004). *Energetic analysis of 24 C20 isomers, Journal of Molecular Structure Theochem* 680,59–63.

Sawtarie, M., Menon, M. and Subbaswamy, K. (1994). *Structure of C20: Bicyclic ring versus cage Phys. Rev. B* 49,7739–7743.

Ternansky, R., Balogh, D. and Paquette, L. (1982). *Dodecahedrane J. Am. Chem. Soc.* 104,4503–4504.

Disch, R. and Schulman, J. (1996). *Heat of Formation of Dodecahedrane J. Phys. Chem.* 100,3504–3506.

Zdetsis, A. (2007). *High-symmetry high-stability silicon fullerenes: A first-principles study Phys. Rev. B* 76,075402 1–5.

Milani, C., Giambelli, C., Roman, H., Alasia, F., Benedek, G., Broglia, R., Sanguinetti, S. and Yabana, K. (1996). *The valence of small fullerenes Chemical Physics Letters* 258,554–558.

Jensen, F. and Toftlund, H. (1993). *Structure and stability of C24 and B12N12 isomers Chemical Physics Letters* 201,89–96.

Guo, T., Diener, M., Chai, Y., Alford, M., Hauer, R., McClure, S., Ohno, T., Weaver, J., Scuseria, G. and Smalley, R. *Uranium stabilization of C28: A Tetravalent Fullerene Science New Series* 257,1661–1664.

Pederson, M. and Laouini, M. (1993). *Covalent container compound: Empty, endohedral and exohedral C28 complexes Phys. Rev. B* 48,2733–2737.

Makurin, Y., Sofronov, A., Gusev, A. and Ivanovsky, A. (2001). *Electronic structure and chemical stabilization of C28 fullerene Chem. Phys.* 270,293–308.

Haneman,D. (1961) *Surface Structures and Properties of Diamond-structure Semiconductors, Phys. Rev.* 121,1093–1100.

Kaxiras, E. (1990). *Effect of surface reconstruction on stability and reactivity of Si clusters, Phys. Rev. Lett.* 64,551–554.

Pandey,K.C. (1981) *New π-bonded Chain Model for Si(111) 2$\times$ 1 Surface, Phys. Rev. lett.* 47,1913–1917.

Himpsel,F.J. and Marcus,P.M. and Tromp,R. and Batra,P. and Cook,M.R. and Jona,F. and Liu,H. (1984) *Structure analysis of Si(111)2 $\times$ 1 with low-energy electron diffraction, Phys. Rev. B* 30,2257–2259.

Lee, S. and Kang, M. (1996). *Model-dependent electronic structure of the Si(111) (2X1) surface Phys. Rev. B* 54,1482–1485.

Xu,G. and Deng,B. and Yu,Z. and Tong,S.Y. and Van Hove,M.A. and Jona,F. and Zasada,I. (2004) *AAtomic structure of the cleaved Si(111)-(2ï£¡1) surface refined by dynamical LEED, Phys. Rev. B* 70,045307–045313.

Ramstad, A., Brocks, G. and Kelly, P. (1995). *Theoretical study of the Si (100) surface reconstruction Phys. Rev. B* 51,14504–14522.

Sun, Q., Wang, Q., Briere, T., Kumar, V. and Kawazoe, Y. (2002a). *First-principles calculations of metal stabilized Si20 cages Phys. Rev. B* 65,235417 1–5.

Li, B. and Cao, P. (2000). *Stable structures for si20 clusters Phys. Rev. A* 62,023201 1–5.

Gao, Y. and Zeng, X. (2005). *M4@Si28 (M=Al,Ga) Metal-encapsulated tetrahedral silicon fullerene The J. of Chem. Phys.* 123,204325 1–4.

Gong, X. (1995). *Stability and electronic properties of nanoscale silicon clusters Phys. Rev. B* 52,14677–14681.

Kaxiras,E. Zeger,L.M. Antonelli,A. and Juan,Y.M. (1994) *Electronic properties of a cluster-based solid form of carbon: C_{28} hyperdiamond, Phys. Rev. B* 49,8446 –8453.

Yu,M. and Wu,S.Y. and Jayanthi,C.S. (2009) *A self-consistent and environment-dependent Hamiltonian for large-scale simulations of complex nanostructures Physica E* 42,1–16.

Ray, C., Pellarin, M., Lerme, J., Vialle, J., Broyer, M., Blase, X., Melinon, P., Keghelian, P. and Perez, A. (1998). *Synthesis and structure of silicon-doped heterofullerenes Phys. Rev. Lett.* 80,5365–5368.

Pellarin, M., Ray, C., Lerme, J., Vialle, J. L., Broyer, M., Blase, X., Keghelian, P., Melinon, P. and Perez, A. (1999). *Photolysis experiments on SiC mixed clusters: From silicon carbide clusters to silicon-doped fullerenes J. of Chem. Phys.* 110,6927–6938.

Martin,N. Giacalone,F. and Prato,M. editors (2009). *Fullerene Polymers: Synthesis, Properties and Applications Wiley .*

M. Pellarin, E. Cottancin, J. Lerme, J.L. Vialle, M. Broyer, F. Tournus, B. Masenelli, P. Melinon (2002). *Coating and polymerization of C60 with carbon : A gas phase photodissociation study J. Chem. Phys.* 117,3088–3097.

Melinon, P., Keghelian, P., Perez, A., Ray, C., Lerme, J., Pellarin, M., Broyer, M., Boudeulle, M., Champagnon, B. and Rousset, J. *Nanostructured SiC films obtained by neutral-cluster depositions Phys. Rev. B* 58,16481–16490.

F. Tournus, B. Masenelli, P. Melinon, X. Blase, A. Perez, M. Pellarin, M. Broyer, A.M. Flanck, P. Lagarde (2002). *Bridging C60 by silicon : towards non-van der Waals C60-based materials Phys. Rev. B* 65,165417 1–6.

Blase,X. Gillet,P. San Miguel,A. and Melinon,P. (2004). *Exceptional Ideal Strength of Carbon Clathrates Phys. Rev. Lett.* 65,215505 1–4.

Hohenberg,P. and Kohn,W. *Inhomogeneous Electron Gas Phys. Rev. B* 136,864–871.

Hohenberg,P. and Kohn,W. (1999). *Electronic structure of matter Rev. Mod. Phys.* 71,1253–1266.

Saito,S. and Oshiyama,A. (1995). *Electronic structure of Si46 and Na2Ba6Si46 Phys. Rev. B* 51,2628–2631.

Moriguchi, K., Yonemura, M., Shintani, A. and Yamanaka, S. (2000a). *Electronic structures of Na8Si46 and Ba8Si46 Phys. Rev. B* 61,9859–9862.

Kohn, W. and Sham, L. (1965). *Self-Consistent Equations Including Exchange and Correlation Effects Phys. Rev.* 140,A1133–A1138.

to be published

Demkov,A.A. Sankey,O.F. Gryko,J. and McMillan,P.F. (1997) *Theoretical predictions of expanded-volume phases of GaAs Phys. Rev. B* 55,6904–6913.

P.Melinon and A. San Miguel (2010). *From silicon to carbon clathrates : nanocage materials Chapter in the vol. "Clusters and Fullerenes" The HANDBOOK OF NANOPHYSICS* Taylor & Francis. (K.Sattler guest editor). ISBN: 9781420075540.

Adams, G., O'Keekke, M., Demkov, A., Sankey, O. and Huang, Y. (1994). *Wide-band gap Si in open fourfold-coordinated clatrate structures Phys. Rev. B* 49,8048–8053.

Melinon, P. and Masenelli,B. (2009) . *Cage-like based materials with carbon and silicon ECS transaction* 13.

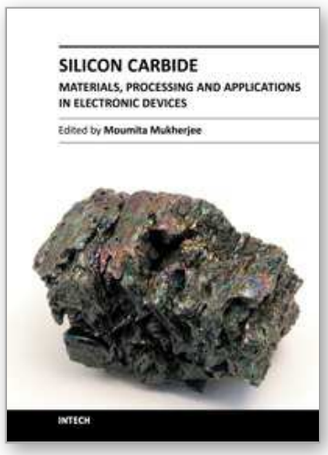

Silicon Carbide - Materials, Processing and Applications in Electronic Devices

Edited by Dr. Moumita Mukherjee

ISBN 978-953-307-968-4
Hard cover, 546 pages
Publisher InTech
Published online 10, October, 2011
Published in print edition October, 2011

Silicon Carbide (SiC) and its polytypes, used primarily for grinding and high temperature ceramics, have been a part of human civilization for a long time. The inherent ability of SiC devices to operate with higher efficiency and lower environmental footprint than silicon-based devices at high temperatures and under high voltages pushes SiC on the verge of becoming the material of choice for high power electronics and optoelectronics. What is more important, SiC is emerging to become a template for graphene fabrication, and a material for the next generation of sub-32nm semiconductor devices. It is thus increasingly clear that SiC electronic systems will dominate the new energy and transport technologies of the 21st century. In 21 chapters of the book, special emphasis has been placed on the â€œmaterialsâ€ aspects and developments thereof. To that end, about 70% of the book addresses the theory, crystal growth, defects, surface and interface properties, characterization, and processing issues pertaining to SiC. The remaining 30% of the book covers the electronic device aspects of this material. Overall, this book will be valuable as a reference for SiC researchers for a few years to come. This book prestigiously covers our current understanding of SiC as a semiconductor material in electronics. The primary target for the book includes students, researchers, material and chemical engineers, semiconductor manufacturers and professionals who are interested in silicon carbide and its continuing progression.

How to reference

In order to correctly reference this scholarly work, feel free to copy and paste the following:

Patrice Mélinon (2011). SiC Cage Like Based Materials, Silicon Carbide - Materials, Processing and Applications in Electronic Devices, Dr. Moumita Mukherjee (Ed.), ISBN: 978-953-307-968-4, InTech, Available from: http://www.intechopen.com/books/silicon-carbide-materials-processing-and-applications-in-electronic-devices/sic-cage-like-based-materials

INTECH
open science | open minds

InTech Europe
University Campus STeP Ri
Slavka Krautzeka 83/A
51000 Rijeka, Croatia
Phone: +385 (51) 770 447
Fax: +385 (51) 686 166

InTech China
Unit 405, Office Block, Hotel Equatorial Shanghai
No.65, Yan An Road (West), Shanghai, 200040, China
中国上海市延安西路65号上海国际贵都大饭店办公楼405单元
Phone: +86-21-62489820
Fax: +86-21-62489821

IntechOpen

IntechOpen